UNIVERSITY OF CALIFORNIA, SAN DIEGO

Symmetry in the retinogeniculate motion circuit

A dissertation submitted in partial satisfaction of the
requirements for the degree
Doctor of Philosophy

in

Neurosciences (specialization in Computational Neuroscience)

by

Alfred Kaye

Committee in charge:

Professor Edward Callaway, Chair
Professor William Kristan, Co-Chair
Professor Tatyana Sharpee, Co-Chair
Professor David Kleinfeld
Professor Terence Sejnowski

2013

The dissertation of Alfred Kaye is approved, and it is acceptable in quality and form for publication on microfilm and electronically:

_____

_____

_____
Co-Chair

_____
Co-Chair

_____
Chair

University of California, San Diego

2013

DEDICATION

To my father, for teaching me to be comfortable with uncertainty.

To my mother, for teaching me to strive for certainty.

To Jennifer, without whom $p(h, m) = 0$.

EPIGRAPH

Cities can be recognized by their pace just as people can by their walk. Opening his eyes, he would recognize it all again by the way the general movement pulsed through the streets, far sooner than any characteristic detail.

—Robert Musil, "The Man Without Qualities"

TABLE OF CONTENTS

LIST OF FIGURES

ACKNOWLEDGEMENTS

Members of the Callaway lab provided technical advice and support throughout the experimental stage of my project, as well as valuable information about the visual system. Jim Marshel was my partner in the experimental work described in Chapter 1 of this dissertation.

Thanks to the members of the Sharpee laboratory for wide-ranging theoretical discussions. Thanks especially to Adam Calhoun, Jeff Fitzgerald, and Ryan Rowekamp, for intellectual stimulation in the first few years of this work.

I am grateful to David Kleinfeld for teaching me optics and for advice and encouragement on decorticated thalamic imaging. Two summers as a TA at Woods Hole under his guidance taught me valuable lessons about statistics, and stimulated some of my best ideas.

Thanks to Tatyana Sharpee, for giving me the freedom and intellectual stimulation to grow as a theorist. Thanks to Ed Callaway for his uncanny knack for knowing what collaboration, question, or push I needed at the right time.

The members of my committee have provided invaluable encouragement, criticism, and advice. I thank them.

Chapter 2, in part, is a reprint of the material as it appears in Neuron 2012; James H Marshel*, Alfred P Kaye*, Ian Nauhaus, and Edward M Callaway. Anterior-posterior direction opponency in the superficial mouse lateral geniculate nucleus. Cell Press, 2012. The dissertation author was the primary investigator and author of this paper. *Equally contributing authors.

Chapter 3, in full, is a preprint of a paper that is being prepared for submission. Alfred P Kaye, Edward M Callaway, Tatyana O Sharpee. Optimal tuning curves for direction selective retinal ganglion cells. In Preparation, 2013. The dissertation author was the primary investigator and author of this paper.

VITA

2004	B. A. in Molecular and Cell Biology (emphasis in Neurobiology) and Comparative Literature, *High honors*, University of California, Berkeley
2008-2012	Graduate Research Assistant, Salk Institute for Biological Studies
2013	Ph.D. in Neurosciences (specialization in Computational Neuroscience), University of California, San Diego

PUBLICATIONS

James H Marshel*, Alfred P Kaye*, Ian Nauhaus, and Edward M Callaway. Anterior-posterior direction opponency in the superficial mouse lateral geniculate nucleus. Neuron, 76(4):713720, November 2012. *Equally contributing authors.

Alfred P Kaye, Edward M Callaway, Tatyana O Sharpee. Optimal tuning curves for direction selective retinal ganglion cells. In Preparation, 2013

ABSTRACT OF THE DISSERTATION

Symmetry in the retinogeniculate motion circuit

by

Alfred Kaye

Doctor of Philosophy in Neurosciences (specialization in Computational Neuroscience)

University of California, San Diego, 2013

Professor Edward Callaway, Chair
Professor William Kristan, Co-Chair
Professor Tatyana Sharpee, Co-Chair

The direction of visual motion is encoded in a population of direction selective retinal ganglion cells (DSRGCs) that provide inputs to the lateral geniculate nucleus (LGN). In this work, a novel method of in vivo two-photon calcium imaging is developed and used to determine how direction selective information is organized in the superficial LGN. Neurons preferring a single direction of motion within the superficial LGN predominantly represent the horizontal directions of motion, and a population of cells exists which responds to both opposing directions along the horizontal axis. A simple statistical model of retina-LGN connections demon-

strates that random wiring within the superficial layer is sufficient to produce the observed fractions of direction and axis of motion preferring LGN neurons. The random wiring model is consistent with previous experimental results on the fraction of LGN neurons receiving a single driving input, and makes quantitative predictions about retina-LGN connectivity.

The efficient coding hypothesis suggests that sensory neurons should be adapted to carry as much information as possible about the statistics of the environment. In a theoretical study, we reconcile this hypothesis with the organization and function of the retinogeniculate motion selective circuit. Under this theory, the symmetries of the distribution of optic flows in natural scenes constrain optimal direction selective neurons to prefer only the cardinal directions of motion. The directional tuning curves of On-Off DSRGCs in mice are compared with the optimal tuning curves for jointly encoding orthogonal directions of motion, and are found to correspond closely. The optimal encoding scheme for two opposing direction selective neurons, as observed in our study of the superficial LGN, requires sharpening of tuning relative the retinal representation. The theory's predicted sharpening corresponds to our own data on direction selective responses in LGN, and predicts that tuning curves that in a vertical motion layer in the LGN should be more broadly tuned than those in a horizontal motion layer.

Chapter 1

Introduction

The visual system of a variety of species computes visual motion from spatiotemporal patterns of light hitting the retina [LMMP59, EB89, BH63, BSNM92]. Visual motion can be used to provide feedback control of movement [WH88, KVD$^+$91], to detect moving objects in the world [LMMP59], and to infer the geometric structure of stationary objects [Adi85]. The function of the early motion pathway in rodents and rabbits, which begins with the computation of motion direction by subtypes of retinal ganglion cells (RGCs) [BH63], has typically been attributed to the reflexive control of eye movements through subcortical brain areas responsible for those movements [Oys68]. The recent discovery that some types of direction selective RGCs (DSRGCs) project to the lateral geniculate nucleus (LGN) in mice [HWE$^+$09] raises the question of how information derived from DSRGCs may contribute to a broader range of visual motion perceptions.

This dissertation addresses the organization of motion selectivity in the mouse LGN and its relationship to the statistics of visual motion in natural scenes. Chapter 1 describes the investigation of direction selectivity in the superficial mouse LGN with a novel vivo two-photon calcium imaging method. Direction selective neurons clustered around the horizontal axis of motion, and a class of neurons selective for both opposing directions of motion along the horizontal axis was observed. A simple probabilistic model demonstrates that these results can be reconciled with random wiring with layers of LGN and predicts quantitative circuit properties. Chapter 2 develops a theory of optimal direction selectivity based on

the efficient coding principle which matches previous experimental observations of ON-OFF DSRGCs as well as the results of Chapter 1. Efficient coding requires direction selective neurons to encode the cardinal directions of motion, and predicts the tuning curve width of ON-OFF DSRGCs. The theory predicts that transformation of opposing directions of motion to produce axis selective neurons should involve sharpening, and that it should only happen for the cardinal axes of motion.

DSRGCs were discovered discovered in the rabbit retina [BH63] shortly after the first direction selective neurons were observed in cats [HW59]. The observation that the On-Off DSRGCs prefer the four cardinal directions [OB67] stimulated work on their mechanism of computing direction selectivity [BL65], function [Oys68, OTC72], and development [EAG$^+$08]. Few studies have attempted to determine the role of DSRGCs in the central perception of visual motion [LOT69, MB69, SCM71, FSSI79], as they were thought to primarily project to subcortical structures involved in reflexive eye movements [OTC72]. Instead, higher order motion features in cortex are thought to receive input from direction selective cortical inputs, which in turn derive their sensitivity to motion from many non-direction selective LGN neurons [SH98].

Since neurons in visual cortex can derive direction selectivity *de novo*, the functional role of On-Off DSRGCs in central vision is unclear. Before delving into our experimental and theoretical work, it is useful to consider the properties of On-Off DSRGCs that set them apart from other direction-selective cells. Each On-Off DSRGC is tuned (responds strongest) to motion in one of the four cardinal directions [OB67]. The neurons responding to a particular direction form a mosaic on the surface of the retina, allowing a complete representation of motion in that direction at each position of the visual field [AO95, HWE$^+$09].

Since the world itself has an overrepresentation of edges in the horizontal and vertical directions, a developmental program could begin with a random assortment of direction preferences and learn to represent the cardinal directions. However, the cardinal motion preference of On-Off DSRGCs is present before eye-opening [WHZF11] and is not altered by dark-rearing or pharmacological manipulations [EAG$^+$08]. Individual subtypes of On-Off DSRGCs preferring a particular

direction have been genetically labeled [HWE$^+$09, KZMS10], further strengthening the claim that any adaptation to the statistics of the natural environment has occurred on an evolutionary timescale.

Oyster and Barlow [OB67] observed that the direction preferences of these neurons corresponded to the extraocular muscles, and thus that they might be involved in the feedback control of eye movements. Oyster [Oys68] suggested that DSRGCs likely "provide errors to a visual servo system which minimizes image motion. To verify this idea, retinal direction information must be traced to its final destination in the brain." In this view, On-Off DSRGCs are a specialized part adapted to a very specific task. Yet with the advent of genetically labelled DSRGC cell lines, it at last became possible to trace these cells to their "final destination." As suggested by Oyster, both ON and On-Off DSRGCs do seem to provide inputs to the anatomical regions responsible for reflexive eye movements. However, On-Off DSRGCs (and also one subtype of OFF-DSRGC) but not ON-DSRGCs were discovered to provide inputs to the LGN [HWE$^+$09, YIS$^+$09].

The principle that the direction preferences of these cells had adapted to the mechanics of the lateral and medial rectus muscles of the eye (controlling eye movements in the cardinal directions) is not disproven by this finding. However, the natural scenes explanation for cardinal motion preference deserves greater consideration. Humans are better at discriminating variability in horizontal and vertical angles than in discriminating oblique angles [App72], and higher order visual areas conserve a bias towards the cardinal directions [LPF03]. Yet widely-used models in which neurons are optimized to discriminate between closely varying directions do not seem to predict the cardinal motion preference (Chapter 2). We present a simple argument from the symmetry of the distribution of visual motion directions in Chapter 2 that predicts the cardinal motion preferences of these cells. The theory can be extended to ask how pairs of neurons should encode visual motion, demonstrating that the On-Off DSRGCs have optimal tuning curves for encoding two orthogonal directions of motion (Chapter 2).

Attention to the On-Off DSRGC pathway in central visual processing grew with the discovery that direction selective neurons in the visual cortex of mice

have a strong bias towards cardinal directions that disappears with experience [RNG+11]. The literature on direction selective neurons in LGN is scant - Levick and colleagues [LOT69] showed that there were direction selective neurons in the rabbit LGN in 1969 and suggested that their tuning curves might be sharpened relative to those of DSRGCs. DSRGCs were observed in the rat [MB69, FSSI79] as well, but cat LGN neurons were found to have only a weak sensitivity to direction [TLZL94].

With the recent discovery that posterior On-Off DSRGCs target the superficial region of the LGN [HWE+09], we became interested in the question of whether it would be possible to observe organization of direction information in the mouse LGN. We developed and applied a novel method of *in vivo* two photon imaging to this problem. The method was depth-limited, but is the first *in vivo* two photon imaging of population activity in the LGN. With this method, we were able to observe the existence of direction selective neurons in the superficial mouse LGN. There was a bias towards horizontal motion preference in the direction selective neurons we observed, confirming the physiological relevance of anatomically observed posterior On-Off DSRGC axons in the superficial LGN [HWE+09]. This anterior-posterior direction opponency was accompanied by an unexpected class of neurons that responded to motion in either direction along the horizontal axis.

We construct a model of random wiring to explain this result in which DSRGC inputs are targeted to different layers but wiring is completely random within a layer. Our intention is to determine whether random wiring could explain the population statistics we observe, or whether it would be necessary to invoke some other mechanisms for LGN neurons to select inputs of a common type. We find that random wiring is sufficient to explain our observations, even when the model is restricted by previous experimental results. Although the model is in agreement with the available data, it paints a picture of LGN wiring in which there is a large degree of integration across functional types giving rise to new feature selectivity such as axis selective neurons. This view of LGN anatomy is at odds with the predominant view of the LGN as a mere relay of retinally derived information [URR99], and is testable with electron microscopy [HHC+04].

The horizontal direction and axis selectivity we observe, and the model we put forward to explain it, further constrains our investigation of the information processing that occurs in the retinogeniculate motion circuit. When pairs of opposing, rather than orthogonal, direction selective inputs synergistically encode visual motion, our theory predicts sharper tuning curves for those cells. Further, the sharpness of tuning in the superficial LGN matches the specific prediction for horizontal preferring neurons, and we make an additional prediction regarding the sharpness of tuning for vertical motion representation.

The statistical symmetries of visual motion thus predict properties of On-Off DSRGCs, and the extension of our theory to encompass the symmetries of the circuit predicts properties of direction selective LGN neurons. As a final step, we generalize our theory to consider a class of neurons responding to both directions of motion along an axis. The distribution of axis of motion can be thought as a doubled circle (Chapter 2, Figure 2.7A) in which some symmetry has been lost with respect to the direction of motion. We show that this symmetry-breaking corresponds to a prediction that oblique axis selective cells are less optimal and more asymmetric than cardinal axis selective cells.

We present results suggesting that there is preservation of symmetry by the retinogeniculate motion circuit. The relationship between circuit, physical, and statistical symmetries in the representation of visual motion underlies this work. Together, these results suggest that the LGN both preserves (by separating into layers) and breaks (by integrating within a layer) physical and statistical symmetries, and that this organization is optimized to transmit information about the direction of visual motion.

Chapter 2

Anterior-Posterior Direction Opponency in the Superficial Mouse Lateral Geniculate Nucleus

2.1 Abstract

We show functional-anatomical organization of motion direction in mouse dorsal lateral geniculate nucleus (dLGN) using the first two-photon calcium imaging of dense populations in thalamus. Surprisingly, the superficial 75μm contains anterior and posterior direction-selective neurons (DSLGNs) intermingled with non-direction-selective neurons, while upward and downward-selective neurons are nearly absent. Unexpectedly, the remaining neurons encode both anterior and posterior directions, forming horizontal motion-axis selectivity. A model of random wiring explainsconsistent with these results makes quantitative predictions about the connectivity of direction-selective retinal ganglion cell (DSRGC) inputs to the superficial dLGN . DSLGNs are more sharply tuned than DSRGCs. These results suggest dLGN maintains and sharpens retinal direction selectivity, and integrates opposing DSRGC subtypes in a functional-anatomical region, perhaps forming a

novel feature representation for horizontal-axis motion, contrary to dLGN being a simple relay. Furthermore, they support recent conjecture that cortical direction and orientation selectivity emerge in part from a previously undescribed motion-selective retinogeniculate pathway.

2.2 Introduction

Visual motion perception depends on the computation of direction of motion from spatiotemporal luminance patterns. It is widely believed that these computations emerge *de novo* in the cortex, independently of retinogeniculate direction-selective inputs [HW61, PLF04]. This view persists in spite of the fact that motion is also computed in the retina [FMW02, WHZF11, BHD11], where subtypes of direction-selective retinal ganglion cells (DSRGCs) encode each of four cardinal directions (On-Off cells) or three distinct directions (On cells). These cells have long been believed to serve purely subcortical pathways and mediate reflexive behaviors [OB67], but not to supply input to cortex.

Recent evidence has begun to challenge the assumption of separate retinal and cortical visual motion pathways in the mouse [HWE$^+$09, KZMS10, RNG$^+$11]. During early development, cortical direction and orientation selective neurons prefer cardinal directions similar to the direction preferences of some On-Off DSRGCS [RNG$^+$11]. After this initial period, direction and orientation tuning evolve into the adult form, characterized by the existence of neurons preferring all directions. This compelling result suggests for the first time the possibility that direction selectivity computed in the retina may strongly influence cortical direction and orientation tuning via a pathway through the dorsal lateral geniculate nucleus (dLGN). However, a functional direction-selective pathway from retina to dLGN to cortex has not been shown in any species. It also remains largely unknown what motion computations, if any, are performed in the dLGN.

In the canonical view, the dLGN simply relays information from the retina to cortex, maintaining segregation of functional cell types as defined in the retina [NC09]. Furthermore, these pathways are generally organized in distinct layers

of uniform functional cell types, perhaps to help maintain segregation of parallel information channels and avoid integration of separate pathways. Thus, if dLGN does relay retinal direction-selectivity to the cortex, it may be organized in distinct layers of uniform function within dLGN. Each cardinal direction of motion is represented by a different type of retinal ganglion cell (RGC), with distinct mosaics across the retina for each DSRGC type [HWE$^+$09]. As such, each direction may be represented by its own layer in the dLGN in order to maintain functional segregation, if the canonical view applies.

Recently, it was shown that at least two On-Off DSRGC subtypes and one novel Off DSRGC type terminate their axons at different depths within the mouse dLGN [KZY$^+$08, HWE$^+$09, KZMS10, REZW$^+$11, KDlHK$^+$11], raising the possibility that there may be a laminar organization of distinct direction preferences in dLGN. Based on the pattern of axon terminals, posterior direction selectivity may be limited to the superficial $\sim$75 μm layer of dLGN and upward and downward direction selectivity may be restricted to deeper layers in dLGN. However, it is not entirely clear from these anatomical studies whether these projections overlap with each other. Furthermore, the projections of anterior and upward On-Off DSRGCs, as well as a multitude of other cell types, have not been traced. Predictions regarding the existence of a laminar organization of direction selectivity in dLGN are further limited by unknown circuit parameters such as whether the relevant dLGN neurons sample from retinal inputs across layers versus near their cell bodies, and the degree to which direction selectivity is preserved across the retinogeniculate synapse. Surprisingly, a thorough electrophysiological study did not report direction-selective or On-Off responses in the mouse dLGN [GT03], bringing into question whether direction selectivity is maintained and relayed at all in mouse dLGN. Although, it is possible that stimulus parameters and analysis criteria of this previous study did not identify direction-selective neurons. Moreover, a functional-anatomical organization of direction tuning has not been shown in any species, despite the rare observation of direction-selective lateral geniculate neurons (DSLGNs) in rats and rabbits [LOT69, MB69, SCM71, FSSI79]. However, the electrophysiological recording methods used by these studies may not

have been able to distinguish the precise depths of a sufficient number of recorded neurons, especially given their rarity in the population (∼5-10%), and potential proximity of some of these neurons to the most superficial layers of dLGN.

Here, we directly examine the functional-anatomical organization of direction tuning in the superficial 75 μm layer of mouse dLGN using the first two-photon calcium imaging of dense populations in the thalamus. This dense sampling of neurons in the superficial LGN allowed us to characterize the direction tuning and precise anatomical location relative to the dLGN surface and border with the lateral posterior nucleus (LP) of dozens to hundreds of neurons simultaneously. By tiling across all three dimensions corresponding to the superficial 75 microns of the dLGN, we sampled hundreds of densely-labeled neurons within the same animal in a given experimental session. The efficiency and thoroughness of this approach distinguishes it from other methods, such as electrophysiological recordings. These advantages of the imaging method allowed us to determine the functional-anatomical organization of motion direction information in the superficial dLGN. We find using this approach that two opposing directions of motion (posterior and anterior) are encoded by subpopulations within the same superficial region. Even more strikingly, we find another comparably sized subpopulation of neurons that encodes both opposing directions of motion within the same neuron to form horizontal axis-of-motion selectivity. All three of these functional subtypes are intermingled within a majority of non-direction-selective neurons within the superficial region. Neurons encoding vertical directions are very rare or nonexistent in this region. We use these findings to examine the likelihood that horizontal direction and axis-selective neurons in dLGN result from locally random integration of concentrated anterior and posterior direction-selective input to the superficial dLGN region.

2.3 Result

2.3.1 Two-Photon Population Calcium Imaging of Visual Responses in Superficial Mouse dLGN

In order to determine the functional organization of direction tuning in the superficial mouse dLGN and test whether direction selectivity follows a laminar pattern of direction preference, we developed a method for in vivo two-photon calcium imaging of neuronal visual responses in the superficial region (leq 75 μm deep from the surface) of mouse dLGN. To our knowledge, these studies yield the first simultaneous physiological measurements of populations of anatomically identified thalamic neurons (Figure 2.1). We expected to find a virtually uniform layer of posterior DSLGNs given axon terminations of posterior DSRGCs specific to this region [HWE$^+$09, REZW$^+$11]. For calcium dye loading, Oregon Green Bapta-1 AM (OGB) was injected into the dLGN of C57/Bl6 mice (Figure 2.1A). To test for direction selectivity in the dLGN, we presented drifting square-wave gratings of 12 equally-spaced directions at a speed known to stimulate DSRGCs [WSH05, KZY$^+$08, KZMS10, HWE$^+$09, YIS$^+$09] (i.e., 25 deg/s, 0.01 cpd). Five repeats of each stimulus and one a blank gray stimulus were presented in random order to the animal while visually-evoked calcium responses were recorded in up to dozens of neurons simultaneously at a known depth in the dLGN, reflecting the underlying changes in firing rate of each neuron [KGH05, KABR10] (Figures 2.1C-1E and 2.2). This method allows even rare neuron subtypes to be detected, and each neurons precise location to be mapped anatomically within the dLGN.

Many neurons responded robustly and reliably to at least one direction of the drifting grating, characterized by a time-locked increase in fluorescence to the period of the drifting grating (n = 353, ΔF/F amplitude at F1 or F2 >2.5% and circular T2 test p <0.05; Figure 2.7). We used the modulation of the fluorescence signal at the temporal frequency of the grating (0.25 Hz, F1) or at twice the temporal frequency of the grating (0.5 Hz, F2) as the measure of neuronal responsiveness. The F1 modulation corresponds to either the onset (On) or offset (Off) of each bar of light passing through a cells receptive field, while the F2 modulation cor-

responds to both the onset and offset (On-Off) of each bar of light. Importantly, since the OGB signal attenuates higher frequencies [VPM$^+$10], a large, detected F2 modulation represents an even stronger than recorded modulation, increasing confidence in On-Off designations. Likewise, an apparently low F2 modulation leaves characterization of On-Off ambiguous or not possible. We computed the direction-selectivity index (DSI) and axis-selectivity index (ASI) of each responsive neuron in our sample. Neurons with high DSI values (DSI >0.5) responded preferentially to a single direction of the grating. Neurons with high ASI values (ASI >0.5) responded preferentially to gratings drifting along a single axis of motion, responding selectively to gratings drifting in either opposing direction along a motion axis at a single orientation. The majority of neurons were not selective for motion in a particular direction or along a particular axis (n = 320/353, Figure 2.2B, DSI <0.5 and ASI <0.5). These responses are consistent with the circular direction tuning curves typical of dLGN neurons [HW61]. These findings demonstrate that the superficial dLGN is far from a purely direction-selective region.

2.3.2 Anterior and Posterior Direction Selectivity in Superficial Mouse dLGN

Conversely, 18 of the visually responsive cells in the dataset were strongly and consistently direction selective (example cells Figures 2.2C, 2.2D and 2.3A, DSI >0.5, Hotelling T2 test p <0.05). The proportion of DSLGNs observed is highly significant compared to chance (shuffled trials, p <10-6, see Experimental Procedures), and is within the range of direction selective fractions previously observed in the mouse retina [KZY$^+$08, HWE$^+$09, BHD11] and rat LGN [MB69, FSSI79]. The majority of neurons in our dataset responded to both the onset and offset of each bar of light moving through their receptive field (n = 10/18), defining their receptive fields as On-Off and strongly suggesting that they receive driving input from On-Off RGCs. The remaining neurons could not be definitively characterized as either On, Off or On-Off. We next tested for functional organization of preferred direction in the superficial dLGN population, based on our predictions from DSRGC projections. Unexpectedly, the majority of DSLGNs were strongly selec-

tive for the anterior direction (n = 11/18, including one near the anterior-downward border, Figures 2.2C and 2.3A), and the majority of these neurons were On-Off direction selective (n = 8/11). Another population of DSLGNs was selective for the posterior direction (n = 5/18, including one near the posterior-downward border), corroborating known posterior DSRGC projections to the superficial layer. At least one of these neurons could be defined with On-Off responses (Figure 2.2D), perhaps reflecting the variety of On-Off response types inherent to that population [HWE$^+$09, REZW$^+$11], and the attenuation of higher frequencies in the calcium signal. Only one neuron was selective for upward motion, and one for downward motion (Figure 2.3A), consistent with rare arborization of On-Off downward and Off upward DSRGC axons in the superficial dLGN layer [KZMS10]. These results strongly predict a previously unknown retinogeniculate projection of On-Off anterior DSRGCs to the superficial dLGN region. Furthermore, insofar as On-Off upward DSRGCs project to dLGN, they are likely to project to deep rather superficial layers.

Overall, the preferred directions of DSLGNs in the superficial 75 μm of the dLGN were distributed along a single axis (Figure 2.3C, axial Rayleigh test, $p < 0.05$, unimodal Rayleigh test n.s.) corresponding to horizontal motion (fitted distribution $<2^\circ$ from horizontal axis). It is important to note that the axial Raleigh test is significant ($p < 0.05$) for DSI thresholds less than 0.5 and greater than 0.22 for neurons which show a consistent direction bias or sensitivity (Hotelling T2 test, $p < 0.05$), suggesting that direction selectivity in the population lies on a continuum (Figure 2.8A). Interestingly, anterior DSLGNs (aDSLGNs) were intermingled in depth with posterior DSLGNs (pDSLGNs) within the superficial 75 μm of the dLGN (Figure 2.3D). The distributions of tuning width between pDSLGNs and aDSLGNs were indistinguishable from each other (t-test n.s.), and were more sharply tuned for direction than reported for DSRGCs [mean width at half-maximum = 76 $\pm$ 7° (SE) for DSLGNs compared to 115° reported for DSRGCs ([EAG$^+$08], t-test $p < 0.05$]. Firing rate to OGB signal transformations are linear at low firing rates [KABR10, LDL$^+$11, NNC12], suggesting that the sharper tuning curves we observe are not artifacts and represent sharpening of direction tuning in the dLGN [see

also [LOT69]]. These results suggest that the dLGN both maintains and sharpens retinal direction tuning in a subset of neurons and contains a preferred direction-biased superficial region. Intriguingly, the direction-selective neurons in this region overwhelmingly encode opposite directions along a single axis of motion.

2.3.3 Horizontal Axis Selectivity

This functional organization of opposing direction tuning prompted us to next investigate whether the dLGN integrates across opposing directions of motion to form axis-of-motion-selective neurons within the same region, in contrast to the role of the dLGN as a simple relay of segregated functional channels. In support of this hypothesis, 15 of the visually responsive neurons were highly selective for a particular axis of motion, at a single orientation of the grating (Figures 2.2E and 2.3B, ASI >0.5). The proportion of ASLGNs observed is also significantly different from chance (shuffled trials, p <10-6, see Experimental Procedures). The preferred axis of motion of these neurons was also overwhelmingly biased towards a single axis (axial Rayleigh test, p <0.05, unimodal Rayleigh test n.s.), corresponding to horizontal motion (Figure 2.3C). The axial Raleigh test is significant (p <0.05) for all ASI thresholds less than 0.5 for neurons which show a consistent axial bias or sensitivity (Hotelling T2 test, p <0.05), suggesting that like direction selectivity, axis selectivity in the population lies on a continuum (Figure 2.8B).

The preferred motion axis for axis-selective neurons was not significantly different than the axis for direction-selective neurons (Watson-Williams test; fitted distribution <20° from horizontal axis). Furthermore, axis-selective lateral geniculate neurons (ASLGNs), pDSLGNs and aDSLGNs were intermingled in depth within the superficial 75 μm of the dLGN (Figure 2.3D; one-way ANOVA n.s.). ASLGNs, like DSLGNs, were more sharply tuned than DSRGCs [mean width at half-maximum = 61 ± 2° (SE) for ASLGNs compared to 115° reported for DSRGCs [EAG$^+$08], t-test p <0.05]. Three of these neurons could be defined as On-Off cells. Cell 1 in Figure 2.2E shows On-Off responses in one such neuron. The similarity in response characteristics of ASLGNs and DSLGNs suggests that they may receive common, retinal input. This is further supported by parameters

of the retinogeniculate circuit, as discussed below.

2.3.4 Random Wiring Model

DSLGNs and ASLGNs in the superficial region both have strong and statistically significant preferences for the same horizontal axis of motion. This suggests that anterior and posterior but generally not upward or downward direction-selective inputs are likely to synapse in the superficial dLGN and that ASLGNs may arise from the integration of opposing direction-selective inputs. This is further supported by the lack of evidence for an axis-selective cell type in the mouse retina (discussed below). Two main hypotheses can explain opposing direction-selective integration to form ASLGNs: 1) horizontal ASLGNs reflect a specific connectivity mechanism that targets certain dLGN neurons or synapses to result in integration of opposing direction-selective inputs, or 2) horizontal ASLGNs reflect integration as a result of random wiring (i.e., random sampling from local axon terminals) in a region which contains axon terminals from both anterior and posterior direction-selective inputs.

In order to determine whether the fractions of DSLGNs, ASLGNs, and non-selective neurons that we observe in superficial dLGN could have arisen by random wiring alone, we developed a simple statistical model of the inputs to the superficial dLGN. The model does not rule out the possibility that other mechanisms contribute to forming this circuit. Rather, it asks whether random wiring alone within the region can explain our findings in a way that is consistent with previous experimental results, and makes testable predictions for future studies. In other words, if the model proves to be valid under these constraints, specific connectivity mechanisms are not theoretically necessary to yield the representation of direction and axis information in the dLGN determined experimentally by our study.

In the random wiring model, neurons receive multiple independent inputs that are anterior DS, posterior DS, or non DS. The random wiring model is constrained by the previous experimental observation that mouse dLGN neurons receive one to three strong inputs from the retina [with probabilities: one input (p_1), two inputs (p_2), and three inputs ($p_3 = 1 - p_1 + p_2$)], from which they derive

their stimulus selectivity [CDL71a, CDL71b, Mas87, Mas92, URR99, CR00]. Importantly, the basic results of the model are robust against the addition of dLGN neurons which receive more than three strong retinal inputs. Inputs from other sources (such as cortex and superior colliculus) are modulatory, rather than driving including in the case of direction tuning [MDCL86, TLZL94]. The model assumes that input from DSRGCs must be nearly pure to generate a DSLGN or ASLGN, since linear summation of inputs only produces direction or axis selectivity (i.e., 0.5 DSI/ASI) if over 90% of the inputs to a cell are of the required type(s). Cleland and colleagues [CDL71a] performed paired RGC-LGN recordings in cats and found that very few (8.8%) LGN neurons had a single RGC input which accounted for all of its spikes, providing information about likely values of p_1. To simulate random wiring, we assume that the probability of input to a dLGN neuron from a given type of RGC is equal to the total proportion of input to superficial dLGN belonging to that RGC type.

Together, these assumptions define a set of equations for each possible type of cell. For example, the probability that a dLGN neuron receives one input and is direction selective is $2p_1f$, where p_1 is the probability of receiving one input and f is the fraction of RGC inputs to dLGN of a single DSRGC type. Other types of cells (e.g., ASLGNs receiving three inputs) can be defined similarly, and the probabilities of each type are shown in Figure 2.6. We assume that the fractions of input to superficial dLGN of either anterior or posterior DSRGCs are equal, and that upward and downward DSRGCs do not project to the superficial region, yielding $2f$ for the total fraction of DS input. The sum of probabilities for observing DSLGNs with one, two, or three inputs in the model is equal to the total fraction of DSLGNs, p(DS). Similar reasoning applies to ASLGNs with two or three inputs, yielding p(AS) (see Appendix for a full derivation). In the model, not all values for p(DS) and p(AS) are possible given random wiring; however the range of possibilities is large (Figure 2.5B, light gray region). Previous studies provide bounds on the likely fraction of dLGN neurons receiving only one driving RGC input ($p_1 = 0.038$-0.19, 95% C.I. derived from Cleland et al 1971 using the Wilson interval for binomial variables with 5/57 single input LGN cells). Applying these

bounds to p1 limits the possible solutions for fractions of ASLGNs and DSLGNs which are consistent with the random wiring model (dark gray region of Figure 2.5B). The experimentally observed fractions of ASLGNs [p(AS) = 0.043, binomial 95% C.I. 0.026-0.069] and DSLGNs [p(DS) = 0.051, binomial 95% C.I. 0.033-0.079] in our dataset (red region of Figure 2.5B) is consistent with the previous data on the limits on p_1 (fall within the bounded region). These results suggest that random wiring is a valid mechanism for yielding the fractions of DSLGNs, ASLGNs and non-selective neurons in the superficial dLGN without violating previous results on the fraction of LGN neurons driven by a single input.

The random wiring model thus defines equations for two experimentally determined values [probability of ASLGN, p(AS), and probability of DSLGN, p(DS)] using three variables (f, p_1, p_2), leaving one free variable. We varied p_2 in order to find the family of solutions for p_1 and $2f$ which satisfy the observed values for p(DS) and p(AS) (Figure 2.5C, black curve with red region indicating confidence intervals). In order for random wiring to explain the experimentally observed axis and direction selective cell fractions, the model predicts that the total fraction of direction-selective input ($2f$) to the superficial dLGN must be between 29 and 39% of the total RGC inputs (25-45% including 95% C.I). The model also predicts that the probability of a dLGN neuron receiving a single, driving retinal input (p_1) is between 0.028 and 0.092 (0-0.167 for the set of p1 values from the 95% C.I of AS and DS fractions, see Experimental Procedures). Importantly, the ranges of $2f$ and p_1 are likely to be much narrower in actuality given that they are based here on the extreme solutions of the model (e.g., $p_2 = 0$), which are very unlikely to occur in the actual circuit. These results predict that the fraction of On-Off DSRGC input to superficial dLGN is similar to the total fraction of retinal ganglion cells that are On-Off DSRGCs, since the fraction of retinal ganglion cells which are On-Off DSRGCs has been estimated to be between 20 and 36% ([HWE$^+$09]; extrapolating for four major On-Off DSRGC subtypes). Also, the range of solutions for p_1 overlap with experimentally observed values determined by dual recordings between retina and dLGN in the cat [Figure 2.5B-C; [CDL71a]]. In this way, our experimental results, combined with the results of our random wiring model and

previous studies suggest that selective connectivity mechanisms are not required in this circuit beyond concentrated anterior and posterior direction-selective input to the superficial dLGN region. Furthermore, the models results given our data make specific predictions about the wiring statistics of DSLGNs and ASLGNs.

2.4 Discussion

These results demonstrate a novel functional organization of opposing direction information in the superficial region of mouse dLGN. The representation of retinal motion information is segregated in terms of horizontal from vertical motion information, but integrated in terms of combining opposing directions along the same horizontal axis within a majority of non-direction-selective neurons in the same region. These dLGN functional cell types likely arise primarily from synaptic integration of retinal inputs. It has been shown that dLGN neurons are strongly driven and highly functionally correlated with their inputs from the retina, which densely synapse on the soma and perisomatic compartments of relay cells [HHC$^+$04]. Moreover, dLGN neurons are modulated, rather than driven, by other inputs such as from cortex, the reticular nucleus and the superior colliculus, which target more distal dendritic compartments [SG98]. Feedback from visual cortex was removed during surgery in the experiment and thus dLGN responses are unlikely to derive from cortex in our experiments (also see [TLZL94]). Projections from the superior colliculus to dLGN have been shown to not drive direction tuning in dLGN [MDCL86]. Thus, it is unlikely that motion-selective responses in dLGN are derived from tuning in the superior colliculus. Furthermore, local connections in dLGN are unlikely to compute direction tuning de novo since excitatory connections are not believed to occur between neurons in the dLGN [CRS03]. However, inhibitory connections do exist within dLGN and may modulate or sharpen direction tuning [LOT69]. It is important to note that excitatory and inhibitory neurons in dLGN were not differentiated by our study. Our results and these previous findings, as well as the known projection of posterior DSRGCs to superficial dLGN, suggest that direction and axis tuning in dLGN are derived

from integration of inputs from the retina.

Accounting for known properties of the retinogeniculate circuit, these results suggest that dLGN can maintain, sharpen and integrate retinal information pathways. Moreover, all of these functions can be accomplished via locally random wiring and do not require uniform functional lamination, as our model shows. Since dLGN provides the majority of sensory input to primary visual cortex, and given the remarkably similar direction preference tuning between retina, dLGN and cortex (present study; [HWE$^+$09, RNG$^+$11]), it is likely that direction tuning first computed in the retina is manipulated by the dLGN and then relayed to cortex. This previously undiscovered pathway may supply motion information to cortex to help derive cortical direction and orientation selectivity. This may indicate a separate mechanism for generating direction and orientation selectivity compared to, in contrast to classic models for the generation of direction and orientation selectivity [HW61, HW62, FM00, PLF04]. Still, like retina, the dLGN likely only represents specific axes of motion, and thus cortex must derive tuning for intermediate directions tuning via additional circuit mechanisms. Future studies will be necessary to reveal whether the retinogeniculate pathway is necessary and sufficient to initiate direction and/or orientation tuning in cortex during development, and what roles the pathway plays in cortical computations, perception and behavior in the adult.

The pattern of direction tuning in superficial dLGN is in agreement with superficially restricted projections of posterior DSRGCs [HWE$^+$09], and deeply restricted projections of On-Off downward and Off upward DSRGCs [KZMS10, KDlHK$^+$11]. Our results suggest that regardless of whether projections of these different DSRGCs overlap, functional segregation is achieved in dLGN. This also strongly implies that DSLGNs sample retinal inputs near their cell bodies, despite having dendrites which likely span across layers, consistent with what has been observed more generally for dLGN relay neurons [HHC$^+$04, SG98]. Furthermore, the results strongly predict projections of On-Off anterior DSRGCs to superficial dLGN and On-Off upward DSRGCs to deep and not superficial dLGN. Similarly, anterior DSRGCs may avoid projections to deep layers, following the pattern of posterior DSRGCs. This suggests a striking model of functional organization in

which the cardinal axes of visual motion are separated in the dLGN (Figure 2.4A). In potential support of this hypothesis, two extracellular recording studies in rats found a similar proportion of DSLGNs compared to the present study, but that >80% of the DSLGNs in their samples preferred motion in vertical-axis directions [MB69, FSSI79], indicating that dLGN encodes vertical directions. These studies did not report precise depths of their recordings, perhaps because of limitations of their methods and the rarity of DSLGNs, but it is likely that their methods tended to sample from deep dLGN and may have largely missed superficial cells. As imaging technologies improve to provide access to deeper dLGN and more DSRGC cell type projections are labeled and characterized, the precise organization of deeper dLGN, and a more complete understanding of potential laminar organization may be revealed. Organizing opposing directions together and separating orthogonal axes in distinct layers represents an unprecedented functional organization for dLGN and may provide advantages for computing higher-order motion parameters.

We observed neurons that encode an axis of motion matching the opposing preferences of direction-selective neurons in the same dLGN region. We see two main possibilities for how this overlap in selectivity arises: either ASLGNs integrate opposing direction-selective retinal ganglion cell type inputs to form a new response class or ASLGNs receive direct input from an undiscovered axis-selective retinal ganglion cell type and relay that information. The latter hypothesis is most consistent with the view of the dLGN as a simple relay from retina to cortex. Interestingly, if this pathway exists it may suggest further specificity of RGC projections based on motion axis preference, for example if vertical axis cells are found in deeper dLGN. However, while axis-selective retinal ganglion cells have been found in the rabbits visual streak [Lev67, VT10], they are nearly absent in the rabbits peripheral retina [Oys68] and have not been described previously in the rodent retina, which has no visual streak. Moreover, while the persistent view has been that the dLGN only relays retinal information and does not generate novel feature selectivity, the current results present the first observed instance of overlapping and opposing information channels in a single dLGN region, and thus

the potential for direct integration of retinal pathways, for example as evaluated by our random wiring model. Interestingly, one previous study suggested potential for rare mixing of RGC type inputs in dLGN to yield intermediate tuning properties of X and Y cells in the cat [Mas92], suggesting that similar mechanisms may be involved in other species and cell types. However, the present results represent the first indication that dLGN may integrate retinal information to form a novel feature selectivity. Regardless of whether axis selectivity first arises in retina or dLGN, the importance of this pathway may be further pronounced if axis-selective inputs influence orientation selectivity in some neurons in the cortexone of the most ubiquitous features represented by the cortex and classically believed to arise in cortex, independent of axis or orientation-selective inputs [HW62, FM00].

Integration of opposing direction preferences by ASLGNs could result from either selective connectivity between DSRGCs and ASLGNs, for example favored by developmental mechanisms, or could occur by chance if connections are non-specific between retina and thalamus, given that incoming axonal arbors of opposing DSRGC types likely overlap spatially within superficial dLGN, as predicted by our results. Future studies are necessary to determine how axis selectivity develops in dLGN. In order to test whether our results are consistent with the generation of ASLGNs by chance integration of DSRGC afferents with opposing direction preferences, we generated a simple model based on random retinogeniculate wiring.

In this model, dLGN neurons receive one to three driving retinal inputs [CR00] randomly distributed according to the fraction of direction-selective inputs from the retina (Appendix). The random wiring model requires that an overwhelming majority (81-100%) of dLGN neurons receive more than one driving input from RGCs in order to produce the proportions of ALSGNs and DSLGNs we observe in the superficial dLGN ($\sim$4% and $\sim$5% respectively). This is consistent with previous studies which have reported that $\sim$92% of relay neurons receive driving inputs from more than one RGC [CDL71a]. The model predicts that a relatively large fraction of RGC input to superficial dLGN is direction selective (>25%),which is similar the fraction of RGCs that are On-Off direction-selective (20-36%, based on anatomical estimates from [HWE$^+$09]). The random wiring model demonstrates

that integration can result by chance from convergence of relatively common direction selective inputs and give rise to the representation of motion we observed (see Appendix for extensions and further discussion of the model). This suggests a developmental mechanism for establishing local concentrations (i.e., lamination) of incoming fibers of specific direction preference, but does not require selective targeting on a single cell basis to generate ASLGNs and maintain direction selectivity in dLGN. If the conditions of the model are not met physiologically, selective wiring between DSRGCs and ASLGNs may be necessary to generate ASLGNs in the absence of direct axis-selective input. Regardless of the mechanism, the juxtaposition of horizontal axis- and anterior-posterior direction-selectivity within the same region suggests a novel computational role for the superficial dLGN. By both sharpening and integrating direction information within a laminar functional organization, the dLGN appears to not merely relay direction information from the retina to cortex, but instead organizes and manipulates that information before projecting it downstream. Future studies examining direct functional connectivity analyzed from the retina to thalamus to cortex, as well as of local interneuron circuits within dLGN may shed light on the mechanisms underlying these computations. For example, whether sharpening of direction tuning in dLGN results from nonlinear postsynaptic summation [CHS07] or precisely targeted feedforward inhibition [WVS$^+$11] remains unknown. The methods developed and demonstrated here in combination with other methods are likely to aid these studies. Furthermore, the influence of these computations and the functional-anatomical organization of direction and motion axis information in the dLGN on visual cortical processing, development and behavior remain intriguing, open questions.

2.5 Methods

2.5.1 in vivo Preparation

All experiments involving living animals were approved by the Salk Institutes Institutional Animal Care and Use Committee. C57Bl/6 mice (n = 7 animals) were anesthetized with isoflurane (1-1.5%). A custom metal frame was

mounted to the skull centered over dLGN stereotaxic coordinates (Figure 2.1A). The frame was a thin round plate, 1 cm diameter and 1 mm thick. A triangular notch in the side of the frame fit into a holding mount that formed a large well around the frame, aided in light shielding, and secured the frame (and mouse) to the optics table. A counterbore in the frame with ∼8 mm diameter formed a small well in the frame and allowed clearance for the objective. A second counterbore with 5 mm diameter served as a notched locator for the custom tubes described below. A 3 mm aperture was centered in the frame. A craniotomy was made within the aperture, and the exposed cortex, including the majority of visual cortex, and underlying hippocampus were aspirated, exposing the thalamus. The brain was rinsed with artificial cerebral spinal fluid (ACSF; in mM: 150 NaCl, 2.5 KCl, 2 CaCl2, 1 MgCl2, 10 HEPES) and a temporary ∼3 mm long cylindrical tube was inserted for stability. A glass pipette was lowered through the cylinder into the dLGN. 10 mM Oregon Green Bapta-1 AM (OGB) with 10% DMSO and Pluronic F-127 [SGHK03] and 50 μM sulforhodamine 101 (SR101) were injected with 150 ms pulses every 15 sec for 15 min at 200 μm below the dLGN surface and again at 400 μm. The temporary tube was replaced with a permanent tube with a glass coverslip sealed to the bottom with index-matched optical glue. This tube was glued in place forming a chamber, which was filled with ACSF. Each of these tubes were shaped as a combination of a cylinder, which was lowered into the brain, and a flat round rim with 5 mm diameter that fit into the frames counterbore, holding it properly in place. OGB-loaded neurons were imaged through the tube using 925 nm excitation with a conventional water-immersion objective (Zeiss 40X, 3.6 mm working distance), attached to the end of a custom-built, light-shielded version of the moveable objective two-photon microscope (Sutter). Images were acquired at 4-8 Hz. This strategy for deep-brain, two-photon imaging was adapted from similar protocols for imaging in the hippocampus [MCSK04, DHT$^+$10]. For visual stimulation, chlorprothixene (1 mg/kg, IM) was administered every 4 hours and isoflurane was lowered to 0.3-0.5%.

2.5.2 Visual Stimulation

Drifting square wave gratings were presented on a calibrated LCD monitor (60 Hz, 34 x 27.5 cm) placed 15 cm from the mouses eye, along an axis parallel to the mouses retina. Gratings were 8 sec duration, 0.01 cpd, and drifted at 25 deg/sec (0.25 Hz) in 12 directions spaced 30 deg apart including: nasal, temporal, superior and inferior, corresponding to anterior, posterior, upward and downward. A blank stimulus was a uniform gray screen and was displayed after every twelve trials. The screen was gray for several seconds between stimulus presentations. For each field of view containing a unique population of neurons, each stimulus was presented 5 times to the animal, in random order, while movies of OGB fluorescence were recorded using the microscope and ScanImage software [PSS03] running on Matlab (Mathworks).

2.5.3 Data Analysis

Each image frame was cross-correlated with a template image to correct for movement. Most trials had only subpixel movements during stimulus presentation. Regions of interest (ROI) were drawn around each cell in each field of view, excluding glia using sulforhodamine 101 labeling [NKKH04], and pixels were averaged within each ROI. The measured fluorescence change relative to a prestimulus baseline ($\Delta F/F$) was calculated and used in all subsequent analyses. Stimulus-evoked response was assessed by taking the Fourier transform of the fluorescence signal at the stimulus frequency (F1; 0.25 Hz in all experiments) and at twice the stimulus frequency (F2; 0.5 Hz). This method has been used to analyze electrophysiological recordings of neurons under periodic visual stimulation since, compared to the mean, it better distinguishes neuronal response classes to periodic stimuli [HS76] and is insensitive to shifts in phase and suppression below baseline. We found this to be true for dLGN calcium responses, and frequency domain analysis provided information about the trial-to-trial reliability of responses used in subsequent analyses. Neurons were classified as visually responsive if they showed an F1 or F2 modulation greater than 2.5%, corresponding to a peak-to-trough height of at least 5%. The circular T2 test [VM91] was used to further restrict our analysis to neu-

rons for which the phase and magnitude of the corresponding Fourier amplitude (F1 or F2) was distinguishable from the blank condition (Figure 2.7, p <0.05).

Five trials were performed at each direction of the grating, and the magnitude of the mean F1 or F2 amplitude was used as the measure of neural responsiveness. Strict criteria for direction selectivity were used, by choosing only those cells which had a Direction Selectivity Index (DSI) >0.5 by both max-null and circular variance metrics:

$$DSI_{max} = \frac{r_{max} - r_{null}}{r_{max} + r_{null}} \tag{2.1}$$

$$DSI_{res} = \frac{|\sum r_k \exp i\theta_k|}{\sum r_k} \tag{2.2}$$

where r_k is the F1 or F2 magnitude at direction k. In order to test for reliability of direction selectivity, the Hotelling T2 test was performed on five resampled resultants ($|\sum r_k \exp i\theta_k|$) to see whether they were distinguishable from the origin at the p <0.05 level. We bootstrapped this p value by generating 1000 samples of five resultants where each resultant has one independent, randomly chosen trial at each direction, and taking the mean p value as the true value. Cells for which F2 or F1 modulation met these criteria were considered direction selective for further analysis, and F2 modulated neurons with F2 >F1 were defined as On-Off. The tuning curves, histograms and response vectors for these On-Off neurons are represented as black in all of the figures. Other neurons (F1 modulated) are represented as red. Despite the low-pass filtering inherent in the spike to calcium transformation, most F2 modulated direction selective neurons had a greater F2 than F1 modulation (n = 6/10).

We then fit each set of responses to a circular Gaussian (von Mises) distribution, which is described as

$$r_{max} \frac{\exp \kappa \cos(x - \mu)}{\exp \kappa} \tag{2.3}$$

and described the tuning width via the relation for the full width at half-maximum

$$FWHM = 2 * arccos \frac{\log(\frac{1}{2}e^{\kappa} + \frac{1}{2}e^{-\kappa})}{\kappa} \tag{2.4}$$

as in [EAG+08]. For population analysis of direction selectivity, the preferred direction of all direction-selective neurons (Figure 2.3A) was transformed by multiplication by 2 in order to map opposing directions onto one another. The resulting distribution was tested for unimodality with a Rayleigh test ($p < 0.05$), and a maximum likelihood fit to a circular Gaussian (von Mises) distribution was used to demonstrate the angle and sharpness of axial tuning (Figure 2.3C). The same procedure was performed for axis-selective neurons (F1 and F2; Figure 2.3B and 2.3C).

In order to determine the probability that the fraction of direction and axis-selective cells we observed occurred by chance (for example from a noisy signal or unreliable neural responses), we resampled individual trials from all of the recorded neuron responses with replacement to generate 10,000 random sets of 60 trials (5 trials per direction, 12 directions), to simulate 10,000 neurons. We then calculated the DSI/ASI and reliability (Hotelling T2 test) for each of these simulated neurons as described in the preceding section, and found that the probability of observing a direction-selective (DS) neuron from chance was $<.001$. In order to determine the probability that we would sample 18 DS neurons by chance, we calculated the cumulative binomial probability for sampling n1 DS F1 and n2 F2 cells, where $n1 + n2 > 17$, in a sample size of 353. The same analysis was repeated for AS neurons. For both DS and AS neurons, the probability of the observed number of selective neurons was $<10\text{-}6$. This suggests that it is highly likely that the AS and DS neurons we observe in dLGN are in fact axis and direction selective. We furthermore calculated 95% confidence intervals for the observed fractions based on the binomial probability distribution (Wilson interval) in order to account for potential biases introduced from sampling from the actual populations of DSLGNs and ASLGNs. The AS and DS confidence intervals defined a range of possible p1 values (0-0.17). Considering the joint 95% confidence interval of p(AS) and p(DS) defined by a multinomial distribution, rather than two independent binomial 95% confidence intervals, produced a similar p1 range (0-0.19).

2.5.4 Random Wiring Model

The random wiring model is described in detail in Appendix: Random wiring model.

2.6 Appendix: Random wiring model

2.6.1 Assumptions

In order to explore whether the observed proportions of direction and axis-selective neurons in superficial dLGN require selective wiring, or whether they could simply arise from random wiring, we considered a model with the following assumptions:

1. Random wiring implies that the probability of an input to a dLGN neuron from a given type of RGC is equal to the total proportion of input to superficial dLGN belonging to that RGC type. To formalize,f_a and f_p are the proportions of anterior and posterior direction-selective RGC inputs to superficial dLGN, respectively. By random wiring, f_a and f_p are also the probabilities that a given dLGN neuron receives input from each cell type, respectively.

2. Mouse dLGN neurons receive 1 to 3 strong inputs from the retina, from which they derive their stimulus selectivity. Previous studies in mice and other species have found that relay neurons typically receive strong input from one to three retinal ganglion cells [CDL71a, CR00]. In addition, the stimulus selectivity of a relay neuron is highly correlated with the stimulus selectivity of its RGC inputs [CDL71b, Mas87, URR99].

3. Any dLGN neuron which receives at least one non-selective RGC input is non-selective. The direction selectivity index (0.5, resultant metric) used in our study would require essentially pure DS input (16:1 ratio DS:non-selective) by linear summation for an output neuron to be classified as DS.

The same rationale applies to axis selectivity. However, note that an output nonlinearity could potentially reduce this ratio.

4. Any dLGN neuron which receives a combination of purely A and P input is axis-selective. Neurons receiving only A and P excitatory retinal input would respond strongly to both directions, indicating axis selectivity. The outcome of the simulation does not weigh heavily on this assumption. For instance, loosening the assumption by allowing some cells to be non-axis-selective under this criterion leaves our primary findings unchanged.

2.6.2 Theory

Under these assumptions, the probability of finding an anterior direction-selective neuron [p(A)] is the sum of the probabilities of observing an anterior DSLGN with one, two and three inputs,

$$p(A) = p(A; n = 1) + p(A; n = 2) + p(A; n = 3) \tag{2.5}$$

where n is the number of inputs. If we take f_a as the probability of a given input being anterior selective (i.e., the fraction of anterior input), then

$$p(A; n = 1) = p_1 f_a, p(A; n = 2) = p_2 f_a^2, p(A; n = 3) = p_3 f_a^3. \tag{2.6}$$

By the first equation, p(A) equals the sum of these probabilities. Similarly, for posterior cells

$$p(P) = p(P; n = 1) + p(P; n = 2) + p(P; n = 3) = p_1 f_p^1 + p_2 f_p^2 + p_3 f_p^3. \tag{2.7}$$

For simplicity, and without altering the results to follow, we take $f_a = f_p = f$, so that the total fraction of direction-selective input is $2f$. The fraction of DSLGNs and ASLGNs neurons generated by one, two and three RGC inputs is given in Supplementary Figure 2.6.

Since the empirical probability of observing DSLGNs (0.05) and ASLGNs (0.04) is known from our experiments, the system of equations

$$p(DS) = p(A) + p(P) = 2p_1 f + 2p_2 f^2 + 2p_3 f^3 = 0.05 \tag{2.8}$$

and

$$p(AS) = 2p_2f^2 + 6p_3f^3 = 0.04 \tag{2.9}$$

has two equations and three unknowns ($p_3 = 1 - p_2 - p_1$). Thus, this system of equations has a single free parameter, which we can write as the probability of two inputs, p_2. Varying p_2,the family of solutions for p_1 and $2f$ are shown in Figure 2.5C.

2.7 Figures

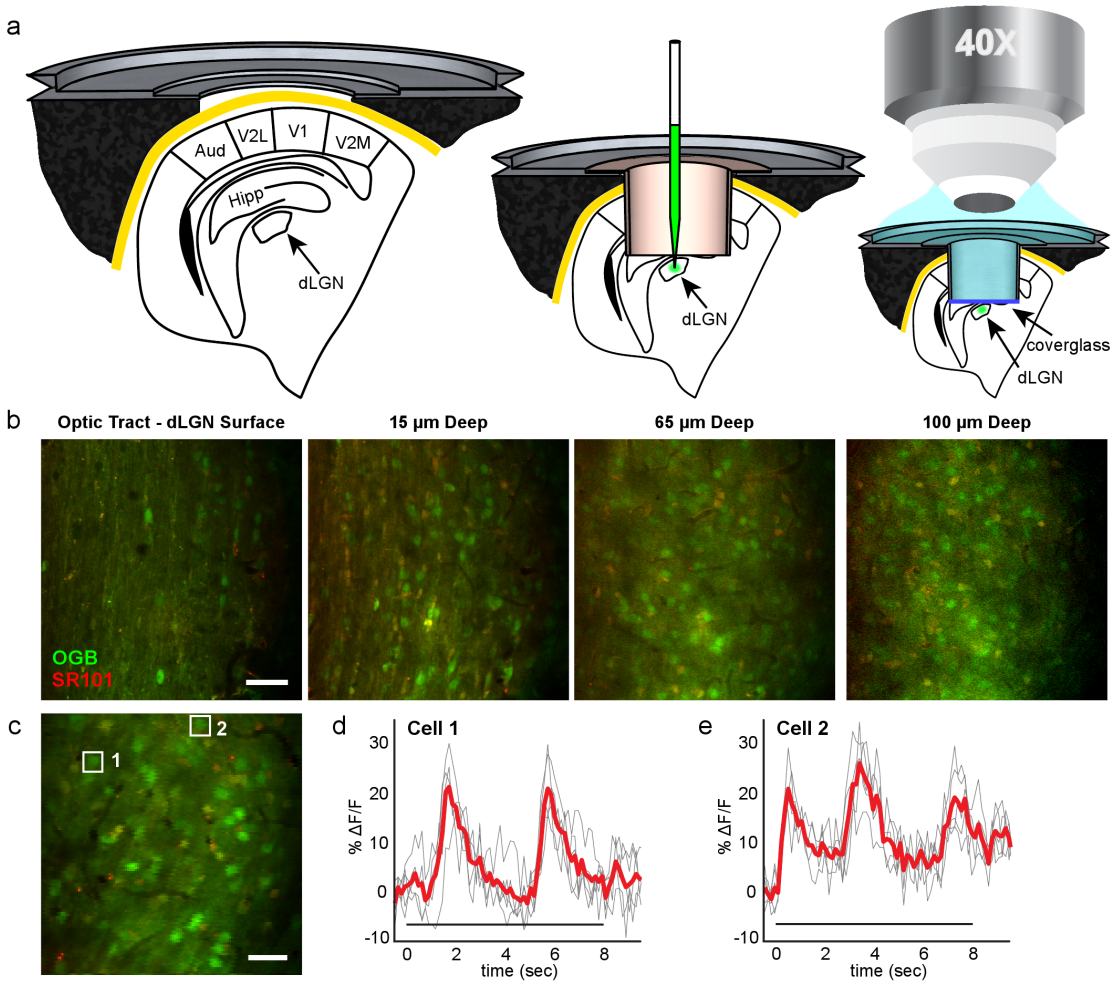

Figure 2.1: (A) Surgery and calcium dye loading procedure as described in Experimental Procedures. Metal frame and tube cross sections, as well as anatomy [**?**] are drawn to scale. The microscope objective drawing is not to scale. (B), Images at multiple depths in the dLGN. Lateral is up. (C), Example field of view used for imaging visual responses. (D-E), Change in fluorescence over time (ΔF/F) for neurons indicated by white boxes in (C). Cell 1 (F1 = 7.6 $\pm$ 0.4% F/F) responds after Cell 2 (F1 = 5.9 $\pm$ 0.7% F/F) indicating slightly shifted positions of their receptive fields relative to the same grating stimulus. Fourier magnitude is unaffected by these shifts in phase (Figure 2.7). Red line indicates mean over five trials; each trial is a gray line. Stimulus time indicated by bar under waveforms. Scale bars: (B), 50 μm (C), 25 μm.

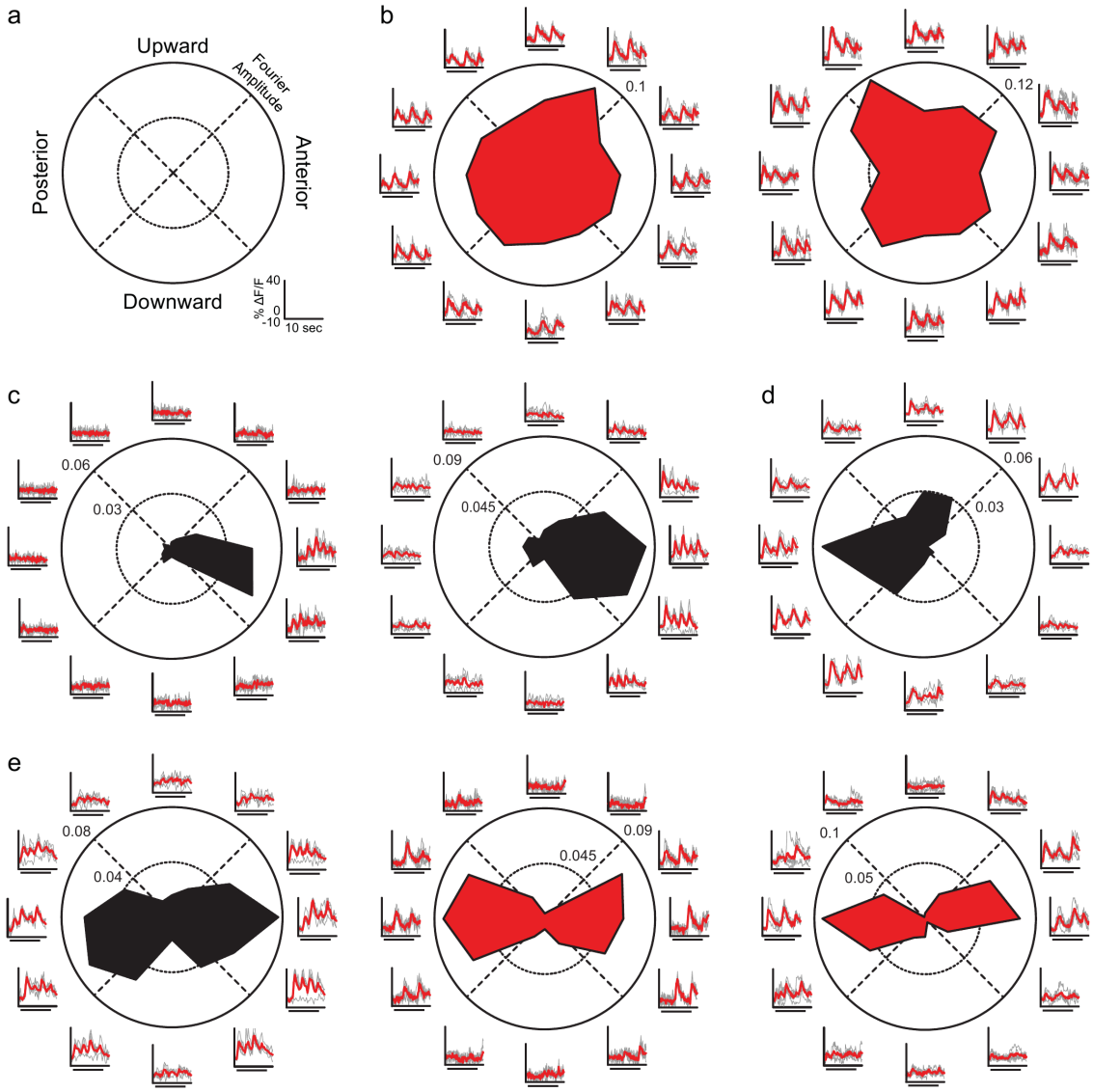

Figure 2.2: (A), Polar plot legend for (B-E), with directions in visual coordinates. Scale bars for fluorescence change ($\Delta F/F$) and time in (B-E) are shown in lower right. (B-E) Examples of non-direction-selective dLGN neurons (B), anterior direction-selective neurons (C), posterior direction-selective neuron (D), and axis-selective neurons (E). Polar plots represent the magnitude of F1 (red) or F2 (black, On-Off) response to each grating direction. Axes outside of the circle show the fluorescence time series, in units of percent change in fluorescence, in response to each direction of the grating. Individual trials (gray) are overlaid with the mean time series (red), where stimulus time (8 seconds) is indicated by bar under waveforms as in (Figure 2.1D-1E).

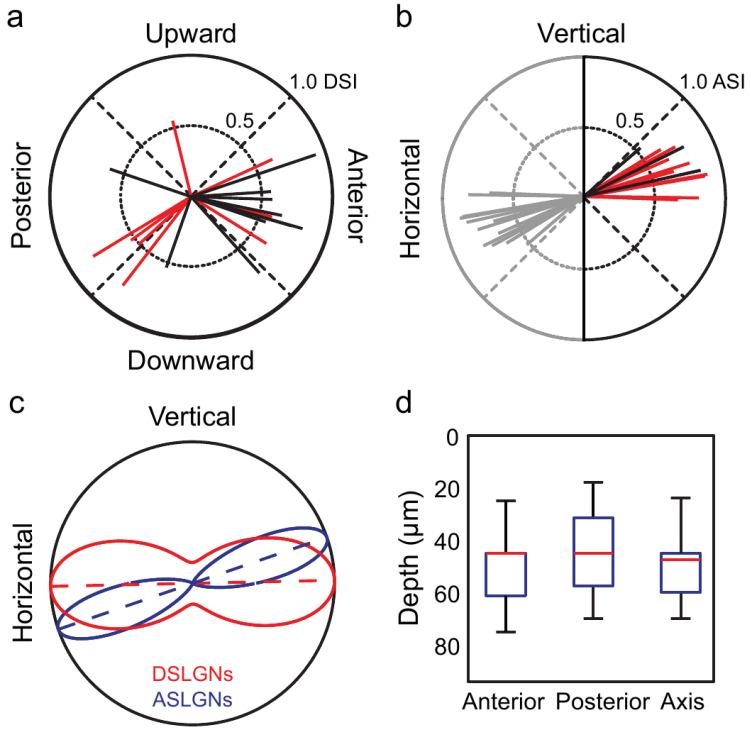

Figure 2.3: (A), Each vector on polar plot indicates a direction-selective neuron. Direction of vector indicates direction preference. (B), Each vector indicates an axis-selective neuron. Direction of vector indicates axis preference. Vectors are reflected (gray) for display purposes, and represent the same data as black and red vectors. (A-B), Length of vectors indicates level of direction selectivity (DSI) or axis selectivity (ASI), using the max-null metric (Experimental Procedures). Data for all neurons in the dataset are shown in Figure 2.8, using the resultant metric and the Hotelling T2 test, for all values of DSI and ASI. Black lines indicate On-Off response (F2 modulation) and red lines indicate F1 modulation. (C), Maximum likelihood fit of axial circular Gaussian distributions to the observed populations of direction- and axis-selective neurons from (A-B). Curves represent the axial Gaussian models probability of observing a direction- (red) or axis-selective (blue) neuron with a given preferred direction or preferred axis. Dotted lines indicate preferred axis for each population, and curves are normalized to equalize the maximum probability density for visualization. Both populations prefer axes representing horizontal motion. (D), Depth of neuron populations in dLGN dataset depending on stimulus selectivity. Whiskers are complete depth range, boxes are 25th to 75th percentile, and the red line is the median depth. Anterior-, posterior- and axis-selective neurons overlap locations in depth within the superficial $\sim$75 μm of dLGN.

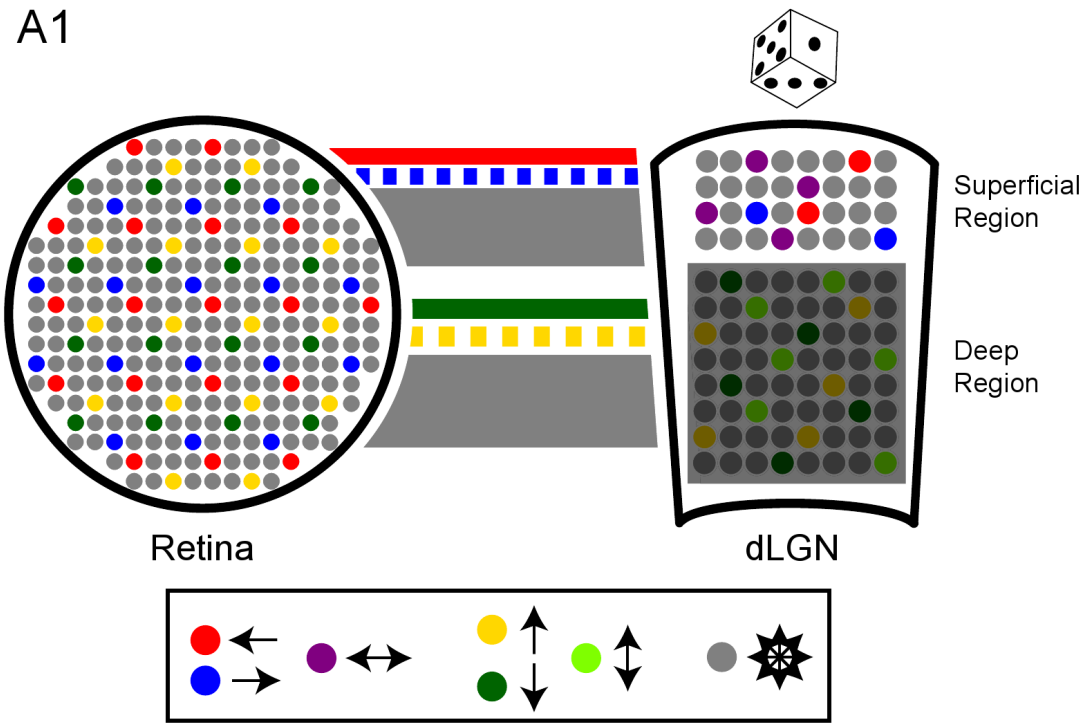

Figure 2.4: (A1) (Left) Mosaics of retinal ganglion cells. Each color represents a different On-Off DSRGC cell type: posterior (red), anterior (blue), upward (yellow), downward (green). Non-direction-selective neurons are gray. (Right, Superficial Region) Organization of dLGN showing the superficial dLGN region containing intermingled populations of posterior (red) and anterior (blue) DSLGNs as well as horizontal ASLGNs (purple) and non-direction-selective neurons (gray) as revealed by the current study. (Right, Deep Region) Predictions for deeper dLGN, including intermingled upward (yellow) and downward (green) DSLGNs as well as vertical ASLGNs (light green). This region is grayed out because its functional organization remains unknown. Lines between retina and dLGN schematics represent RGC axons. Color conventions are same as rest of figure. The thickness of the lines indicates predicted fraction (f) of overall input from our random wiring model. Solid red and green lines represent known projection patterns of posterior and downward DSRGCs, respectively, whereas dashed blue and yellow lines represent predicted projection patterns of anterior and upward DSRGCs made by the current study. Our random wiring model demonstrates that concentrated, laminar projection patterns of opposing DSRGCs can yield the fractions of DSLGNs and ASLGNs we observe in superficial dLGN given locally random wiring.

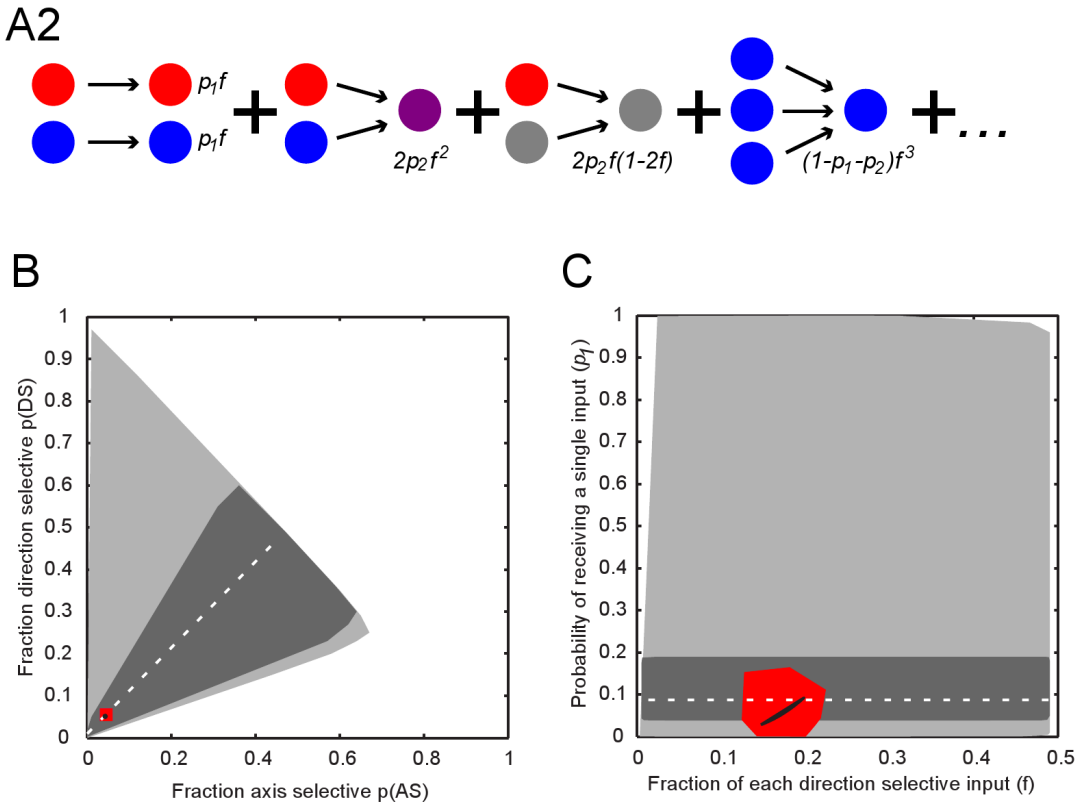

Figure 2.5: (A2) Basic probabilistic theory of the model which assumes dLGN neurons receive one (probability = p1), two (p2) or three inputs (1-p1-p2) from retina that drive their selectivity, including a variable for the fraction of anterior and posterior direction selective input (2f). Some examples of individual probabilities are shown. See also Appendix and Figure 2.8 as well as the main text for details of the model. (B, C) Results of the model. (B) All possible ASLGN and DSLGN fractions based on the model without further constraints (light gray area). The fraction of purely single input neurons from [CDL71a] (95% binomial C.I.: dark gray area 0.038 <p1 <0.19, actual value: dotted line) constrains the model. The observed fractions of ASLGNs and DSLGNs in our study (95% binomial C.I. from Wilson interval: red area, actual value: black dot) falls within this plausible range. (C) Possible p1 and f values (by varying p2) corresponding to the differing constraints in (B): unconstrained model (light gray region), constraining p1 to be consistent with the fraction of purely single input neurons from [CDL71a] (95% C.I.: dark gray region, actual value: dotted line), or constraining the model to be consistent with the experimentally observed ASLGN and DSLGN fractions in this study (95% C.I.: red region, actual value: black curve).

	1 input	2 inputs	3 inputs
DS outcomes	A, P	AA, PP	AAA, PPP
Probability	$p(DS;1) = 2p_1 f$	$p(DS;2) = 2p_1 f^2$	$p(DS;3) = 2p_3 f^3$
AS outcomes	$\emptyset$	AP, PA	APA, AAP, APP, PAA, PAP, PPA
Probability	$p(AS;1) = 0$	$p(DS;2) = 2p_1 f^2$	$p(AS;3) = 6p_3 f^3$

Figure 2.6: Non-selective inputs would render dLGN neurons non-direction-selective (DSI <0.5) in almost all instances, reducing possibilities to two permutations that are DS for each number of inputs. AS cells can only be produced from two or more inputs.

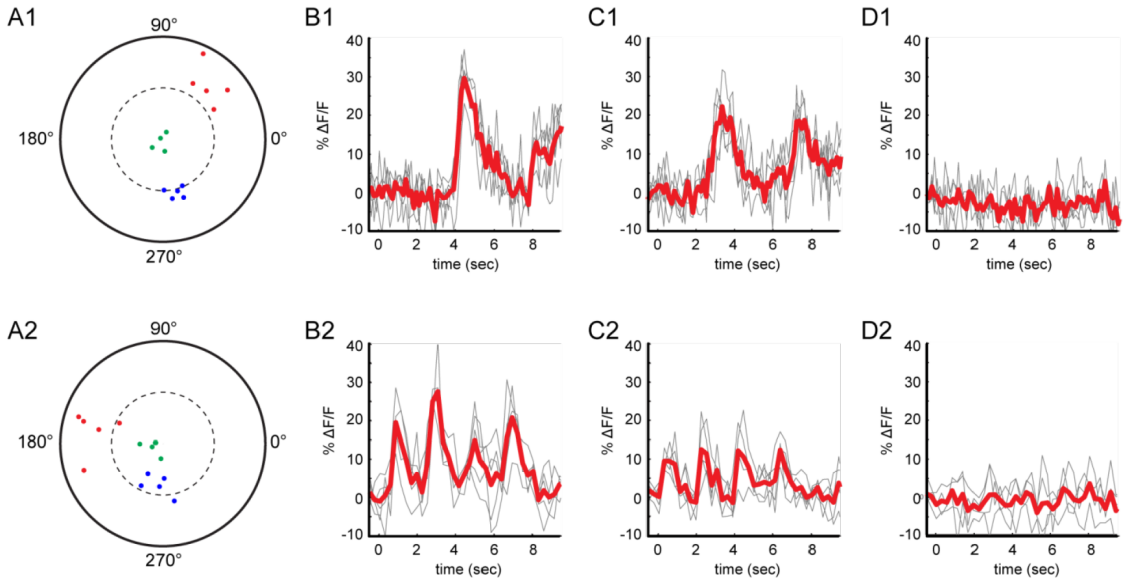

Figure 2.7: (A1-D1) F1 modulated neuron. (A2-D2) F2 modulated neuron (On-Off cell; F2 >F1). (A1 and A2), Polar plot shows phase (angle) and magnitude (radius, with inner circle 6% and outer circle 12% ΔF/F) of F1 modulation for individual trial responses to drifting gratings at 180 degrees (blue dots) and 0 degrees (red dots), and to a blank gray screen (green dots) for (A1), and F2 modulation for individual trial responses for a different neuron to drifting gratings at 0 degrees (red dots), 300 degrees (blue dots) and to a blank gray screen (green dots) for (A2). The circular T2 statistic [VM91] is used to determine the probability that a response at a given direction overlaps with the response to the blank, and is derived from the ratio of the variance within conditions (chosen direction or blank) to the variance between conditions (distance between chosen direction and blank). Note that the response magnitude used in defining direction selectivity is defined to be the distance between the origin and the center of a particular cloud of points. (B1-D1) Fluorescence time series of F1 modulated neuron showing individual trials (gray) and mean responses (red) to drifting gratings at 180 degrees (B1), drifting gratings at 0 degrees (C1) and gray screen (D1). (B2-D2) Fluorescence time series of F2 modulated neuron showing individual trials (gray) and mean responses (red) to drifting gratings at 0 degrees (B2), drifting gratings at 300 degrees (C2) and gray screen (D2).

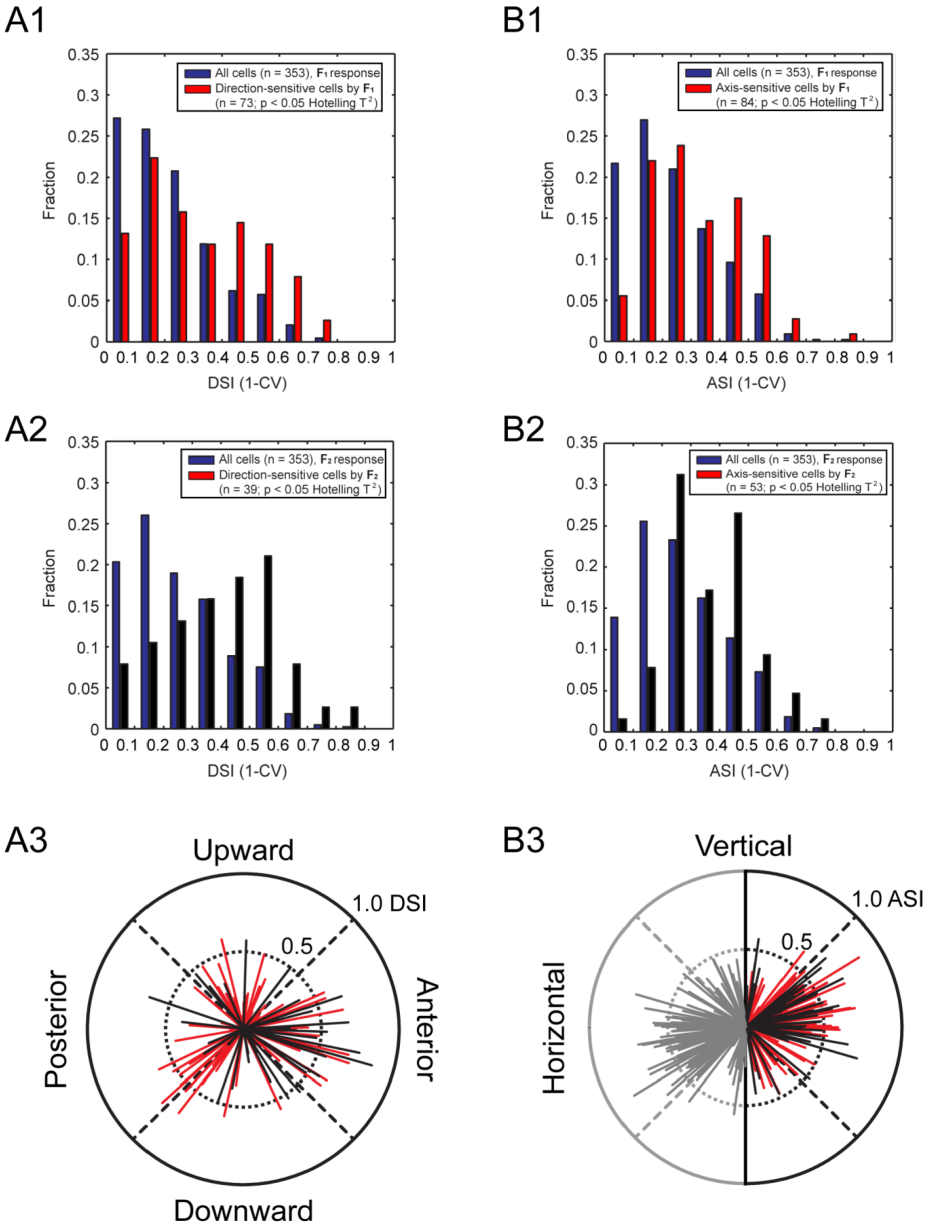

Figure 2.8: (A1-A2) Distribution of DSI for all neurons (blue, A1-A2) by F1 (A1) and F2 (A2) metrics, and for direction-biased neurons (Hotelling T2 test, p <0.05) by F1 (red bars, A1) and F2 (black bars, A2). (A3) Preferred directions (angle of vectors) for all neurons with a significant bias for a direction (Hotelling T2 test, p <0.05). (B1-B2) Distribution of ASI for all neurons (blue, B1-B2) by F1 (B1) and F2 (B2) metrics, and for axis-biased neurons (Hotelling T2 test, p <0.05) by F1 (red bars, B1) and F2 (black bars, B2). (B3) Preferred directions (angle of vectors) for all neurons with a significant bias for an axis (Hotelling T2 test, p <0.05). The magnitude of each vector is the DSI or ASI value. Vectors are reflected (gray) for display purposes in (B3), and represent the same data as black and red vectors.

Chapter 2, in part, is a reprint of the material as it appears in Neuron 2012; James H Marshel*, Alfred P Kaye*, Ian Nauhaus, and Edward M Callaway. Anterior-posterior direction opponency in the superficial mouse lateral geniculate nucleus. Cell Press, 2012. The dissertation author was the primary investigator and author of this paper. *Equally contributing authors.

Chapter 3

Optimal tuning curves for direction selective retinal ganglion cells

3.1 Abstract

Subtypes of retinal ganglion cells encode the direction of visual motion of objects in the world. The efficient coding hypothesis holds that this encoding should be optimized for the natural statistics of motion [BR61]. Fisher Information optimal theories predict that neurons should be more sharply tuned than is observed [ZS99], do not match the observed direction preferences of retinal ganglion cells, and do not naturally take into account synergies when multiple neurons jointly encode the same variable [BN98].

We present an information-theoretic theory of optimal direction selectivity for encoding natural optic flow distributions that reconciles features of retinal motion processing with the efficient coding hypothesis. The direction preferences of optimal neurons correspond to symmetries in the stimulus distribution, explaining the cardinal motion preference of On-Off direction selective retinal ganglion cells (DSRGCs) [OB67], in contrast to previous theories. Extension of the theory into the problem of population coding shows that the tuning width of On-Off DSRGCs

[EAG+08] is optimal for the representation of two orthogonal directions of motion, an organization that can produce unbiased estimators of direction [VH90]. In contrast, the joint encoding of opposing directions of motion requires sharper tuning, as has been observed in direction selective neurons of the LGN [LOT69]. This prediction is consistent with observed characteristics of the mouse LGN, where a sharpened joint encoding of two opposing directions of motion has been observed [MKNC12]. There is also a novel prediction that vertical motion opponency should result in less sharply tuned cells than horizontal motion opponency, due to anisotropies in the natural optic flow distribution. On-Off DSRGCs in the mouse retina transmit as much information as possible about the distance from their preferred direction. A simple theory explains the cardinal motion preference of these cells [LOT69, MKNC12] as well as the transformation of directional information that occurs in the retinogeniculate synapse. The theory explains not only physiological but also anatomical aspects of this circuit, and provides a framework for future analyses of more complex motion features [RNG+11]. A generalization of the theory to encompass adaptive binning provides insight into the relationship between the observed asymmetry of orientation tuning curves [HA78, Swi98] and the stimulus distribution.

3.2 Introduction

Both computer and neural vision systems use apparent motion to infer the changing geometric structure of the world [Adi85, KH96, WH88]. The optic flow representation, in which visual motion is reduced to a motion vector at each visual field position, enables the subsequent computation of that geometric structure [WH88]. Self-motion through the natural world produces a statistical distribution of optic flows, and the efficient coding hypothesis holds that the neural encoding of optic flows should be optimized for this natural distribution [BR61]. In some mammals, the encoding of optic flows takes place in retinal ganglion cells (RGCs) which respond selectively to visual motion in a particular direction [BH63]. These direction selective retinal ganglion cells (DSRGCs) have become a canonical circuit

for considering how simple and sparse synaptic connections between neurons can perform complex sensory computations [BHD11, WHZF11]. A genetic program establishes a complete optic flow representation through four subtypes of On-Off DSRGCs [EAG+08, HWE+09], each of which disregard the brightness of an object and instead respond to its motion in one of the cardinal directions [OB67].

Although recent evidence suggests that On-Off DSRGCs may help shape direction selectivity in cortex [RNG+11], models of cortical direction selectivity predict it developing from non-selective retinal and thalamic inputs [Hee93]. Physiology experiments in visual cortex have therefore been used to constrain computational models of how neurons compute direction selectivity [Hee93, MU81]. These models seek to explain how selectivity for complex motion features (e.g., the global optic flow corresponding to moving forward at an angle of 40°) are constructed from hundreds or thousands of local direction selective inputs [DW91], or how those local direction selective inputs derive from LGN inputs [MU81]. In contrast, feedforward processing of On-Off DSRGC signals occurs in the LGN [LOT69, HWE+09, KZMS10], where a small number of relatively large retinal inputs shapes motion selectivity [CR00, MKNC12]. Each direction selective retinal input is broadly tuned [EAG+08] and represents a cardinal direction [OB67], which further constrains the computation that occurs at this synapse.

At the retinogeniculate (RGC-LGN) synapse, the representation of motion is transformed [MKNC12] before being transmitted to a subsequent stage of processing (visual cortex). The feedforward model of visual neuroscience consists of a sequence of such computations, each constructing neurons that respond to a more complex visual feature than the previous stage [FE91]. Unlike cortical stages of processing, retinal direction selectivity derives from a simple anatomical circuit producing asymmetric inhibitory inputs from a single class of cells (starburst amacrine cells), which has been demonstrated with both electron microscopy [BHD11] and paired intracellular recordings [WHZF11]. Similarly, On-Off DSRGCs preferring different directions appear to project to subregions of the LGN [HWE+09, KZMS10], suggesting a sparse input pattern that is in keeping with known features of the LGN [CR00]. In a separate work, we found evidence for

this model of direction selectivity in the LGN using two-photon calcium imaging [MKNC12].

The present work reconciles the retinogeniculate motion circuit with the efficient coding hypothesis by predicting observed features of the circuit from the probability distribution of natural optic flows. The theory provides an explanation for the tuning properties of the motion circuit, and makes predictions for future studies of the subsequent stages of processing of motion. More broadly, the framework provided here is relevant to the encoding of any circular variable by neurons, such as phase coding of interaural time differences [CK90], motor direction [AG00], or whisker deflection [SBA03]. The encoding of directional variables by neurons is a fundamental problem, and has especially been considered with reference to the discriminability of direction of motion in the presence of noise [SBNM96]. Theories using the Fisher Information have be used to determine optimal neural tuning curves for this discriminability task [ZS99, SS93], and have been shown to match properties of direction selective neurons in visual cortex [GS10]. van Hateren found that the perpendicular, cosine tuning curves observed in blowflies produce a non-biased estimator of the direction of motion [VH90], although the DSRGC tuning curves are not cosine shaped [EAG$^+$08]. The present study makes use of the natural distribution of optic flows to extend this result, showing that the optimal tuning curves are not only perpendicular but specifically prefer the cardinal directions. In addition, we show that On-Off DSRGC tuning curve widths are optimal for a representation of perpendicular directions, but that the LGN appears to transform these tuning curves in order to optimally represent opposite directions.

3.3 Results

3.3.1 Optimal direction preference

Optic flow fields are computed from sequences of images in time [HS81]. In the process, a time series of luminances within a region of space becomes a single circular variable, the direction θ of motion within that region, which is not uniformly distributed in the natural environment. In order to determine whether

the DSRGC encoding is statistically optimal for encoding optic flows, the distribution of optic flows in the natural environment is needed. We used the CatCam video dataset [BEKK04] of cameras mounted on cats as they explored a natural environment to derive the probability of flow in each direction, $p(\theta)$ (Figure 3.1A).

$p(\theta)$ was well approximated by a symmetric double Laplacian distribution (Pearson's $\rho^2 = 0.95$; Materials and Methods) with a marked preference for horizontal over vertical motion. The form of this distribution and observed symmetry is similar to that observed in Roth and Black's (2005) [RB05] study of flows induced by human camera operators (although they observed greater upward than downward motion). The two-fold symmetry of $p(\theta)$ (Figure 3.1A) was robust to variation of the standard deviation of the Gaussian kernel and the threshold. The interplay between scene structure and ego-motion gives rise to this optic flow distribution [CL07], which in turn is represented by motion selective neurons. The directional tuning curves of DSRGCs, following the efficient coding hypothesis, should therefore be matched to $p(\theta)$.

Specifically, the efficient coding hypothesis holds that neurons should carry as much information as possible about the stimulus. An individual neuronal tuning curve, $r(\theta)$, should maximize the mutual information

$$I(r;\theta) = H(r) - H(r|\theta), \tag{3.1}$$

where $H(\cdot)$ is the entropy, or uncertainty, of a probability density. In the low noise limit ($H(r|\theta) \approx 0$), the optimal tuning curve is one which matches its gain to the probability of a stimulus, $|r'(\theta)| = p(\theta)$ [Lau81]. For neurons encoding linear variables, the optimal response functions are just cumulative distributions of the stimuli. However, when the stimulus is a circular variable (i.e., angle), the optimal response functions cannot simply be defined as cumulative distributions, since this would lead to discontinous responses (a neuron responds weakly to 0°, and strongly to 359.9°).

This apparent paradox can be resolved by considering which stimulus features are encoded by direction selective neurons. Equation 3.1 corresponds to the amount of information conveyed by the neuron's activity about the entire range of stimulus directions. The neuron may carry more information about its preferred

direction or about some other direction, based on the stimulus distribution and its tuning curve. Remarkably, a symmetric direction selective tuning curve can maximize $I(r;\theta)$ only when the preferred direction lies along an axis of symmetry of $p(\theta)$, since the two halves of $r'(\theta)$ are equal to $p(\theta)$. This argument is developed in detail in the Appendix to this chapter and extended to the case of neurons responding to both directions along an axis (Supporting Figure 3.4).

The conventional view of direction selective neurons is that they communicate a very specific behaviorally relevant signal about the likelihood that motion is occurring in their preferred direction [BSNM92] for use in an ethologically relevant behavior. To optimally accomplish these tasks, direction selective neurons would have to maximize the information between the neural response and how far the angle of visual motion is from the neuron's preferred angle, $\delta\theta = |\theta - \theta_{max}|$. Higher information between $\delta\theta$ and the neural response $I(r;\delta\theta)$ would make it possible for a feedback control system, for example, to better determine whether motion occurs in that direction. An optimal neuron, for the purposes of this study, is one that both communicates as much information as possible about $\delta\theta$ in addition to carrying as much information about θ,

$$\underset{r(\theta)}{\text{argmax}} I[r(\theta);\delta\theta] = \underset{r(\theta)}{\text{argmax}} I[r(\theta);\theta]. \tag{3.2}$$

There is a unique tuning curve that is both direction selective and maximizes $I(r;\theta)$ for every preferred direction (Materials and Methods). Surprisingly, these tuning curves are not symmetric unless the preferred direction lies along an axis of symmetry of $p(\theta)$ and they do not maximize $I(r;\delta\theta)$ (Figure 3.1C). The bilateral symmetry of $p(\theta)$ constrains optimal direction selective neurons to prefer only the four cardinal directions, corresponding to the horizontal and vertical axes of symmetry. The On-Off DSRGCs differ from other classes of retinal directions selective cells as well as cortical direction selective neurons in fulfilling this criterion for optimality.

This prediction is not generated by the overrepresentation of motion in the cardinal directions (i.e., peaks in the distribution), but rather by the symmetries of the stimulus distribution. Asymmetric directional tuning curves maximizing $I(r;\theta)$ are locally optimal in that the gain matches the stimulus distribution, but

globally suboptimal in they introduce ambiguity between the distance from the preferred direction and the neural response. This uncertainty, or noise entropy $H(r|\delta\theta)$, reduces the information transmitted by the neural response about the distance from the preferred direction.

Every value of the neural response can be produced by two different directions on the tuning curve. Optimal direction selective neurons occur when these two directions occur at the same distance from the preferred direction, which occurs only for the cardinal direction preferring curves.

For comparison, the Fisher Information $\mathcal{F}$ [ZS99, SS93] provides a different optimality criterion which predicts that neurons should place the highest gain (largest $r'(\theta)$) at those regions where the probability of the stimulus is maximal. The optimal preferred directions in the Fisher scheme are not the most likely stimuli - rather, they are the preferred directions for which the sharpest part of the tuning curve is at the horizontal axis (Figure 3.1D). As the sharpness of tuning increases, this causes a split into four discrete optimal preferred directions, but the optimal direction selective neurons are rotated from the cardinal direction representation of On-Off DSRGCs [OB67] and the efficient coding theory.

The average $\mathcal{F}$ is highest for infinitely sharp tuning curves [ZS99, SS93], so it does not provide a meaningful prediction about what the sharpness of tuning should be. Furthermore, the Fisher Information is additive in the number of neurons present, so that it doesn't provide a measure of neural encoding which encompasses synergistic encoding of stimuli. For large populations, it is possible to add additional constraints on the encoding [GS10] or noise correlations between neurons [ZS99] to obtain predictions, but this precludes the sort of analysis of pairs of highly specific encodings that are relevant to the processing of information contained in On-Off DSRGCs and introduces additional assumptions.

3.3.2 Pairs of direction selective responses

The feedforward circuit from retina to LGN is organized so that one to three strong inputs drive each relay cell [CR00, HHC$^+$04]. Our own experimental results indicate that there may be neurons in the LGN which receive driving inputs from

two direction selective neurons preferring different directions [MKNC12]. Recently, the discovery of a dramatic bias towards the cardinal directions amongst direction selective neurons in the mouse visual cortex has raised the possibility that information from On-Off DSRGCs may be pooled in the cortex as well [RNG$^+$11]. The remarkable sparsity of the LGN circuit prompted us to consider the problem of how multiple direction selective neurons should jointly encode object motion. We extended the maximum response entropy framework to the case of two neurons, in the case where both neurons are encoding the same stimulus parameter θ.

Optimal direction selective neurons exist when information betweeen the neuron's response and the both the angle of motion and the difference between that angle and a preferred direction are maximized (equation 5). Neurons thus derived are not necessarily Fisher optimal, since $\mathcal{F}$ will be maximized by neurons putting the maximum values of $r'(\theta)$ at the points where $p(\theta)$ is highest (Figure 3.1C). Extending Fisher Information theories to the case of multiple neurons requires additional constraints (e.g. on neuron density, etc.) or the introduction of explicit noise correlations to capture synergistic encoding of stimuli, since $\mathcal{F}$ is additive in the number of neurons. Synergistic encoding incorporates naturally into the mutual information, in contrast, and surprisingly matches observed features of the retinogeniculate motion circuit.

In the absence of noise, the trajectory of two direction selective neurons responding to different directions of motion (Figure 3.2A)will therefore be a curve (1d manifold) in a 2d firing rate space (Figure 3.2B). Integrating over the path described by this curve yields the response entropy,

$$H(\vec{r}) = \int p(\vec{r}) \log p(\vec{r}) d\vec{r} \tag{3.3}$$

We can decompose the response entropy into the entropy due to the stimulus and an additive term, the line entropy, which is equal to the average log of $\mathcal{F}$,

$$H_{\text{response}}(\vec{r}, \theta) = H(\theta) + \underbrace{\frac{1}{2} \int d\theta p(\theta) \log[r_1'^2 + r_2'^2]}_{\text{Line entropy}} \tag{3.4}$$

The line entropy provides the contribution of the direction selective tuning curves to the encoding, since the stimulus entropy is independent of the response func-

tions. Unlike the Fisher Information [ZS99], this term is not additive and thus is sensitive to the synergistic encoding of direction by a pair of neurons.

Two orthogonally tuned direction selective responses enable the unbiased estimation of all directions of motion [VH90]. A pair of orthogonal direction selective neurons maximizes response entropy relative to the empirical stimulus distribution when the sharpness of each tuning curve is 118°(Figure 3.2C). This maximum is well-defined and corresponds to an optimal encoding in the absence of noise or in the presence of additive Gaussian noise in the responses (see Materials and Methods). The theory gives us a geometric insight into the reason for this maximum - this value corresponds to the longest trajectory in r_1-r_2 space (red trace, Figure 3.2B). Remarkably, the tuning width of On-Off DSRGCs in the mouse retina is 120° [EAG$^+$08], almost exactly equal to the tuning width at which the information between the neural response and the stimulus is maximized.

The optimal tuning width for pairs of direction selective neurons is highly dependent on the distance between the preferred directions of the neurons (Figure 3.3). The tuning width of On-Off DSRGCs would therefore not be optimal for pairs of direction selective neurons separated by either 45 or 180°. As the distance between the pair of neurons' preferred directions increases, the neurons must become sharper according to this result. A sharpening of On-Off DSRGC output has previously been observed in the rabbit LGN [LOT69]. Data from our own experiments, published separately from this work, show that in the mouse LGN, there exists a layer of opposing horizontal direction selective neurons in the superficial LGN. The theory predicts that if this region is truly optimized to represent opposing horizontal directions, significantly sharper tuning should be observed relative to the retina. In fact, just such a sharpened tuning was observed (FWHM 76 $\pm$ 7° SEM), and the degree of sharpening precisely matched the prediction of the theory for horizontal but not vertical neurons. These results also point to a potential anisotropy between the vertical and horizontal directions, in that a pair of opposing vertical direction selective neurons should be significantly less sharp than the neurons in the horizontal layer. This prediction would obviously not hold for pairs of direction selective neurons that were not optimized to the natural optic

flow distribution (Figure 3.3).

3.4 Discussion

On-Off DSRGCs create a representation of the retinal direction of movement at each location in visual space - that is, they represent optic flow. These cells respond invariantly to the polarity of the stimulus [BH63], and are not built out of intrinsically orientation selective subunits like DS cells in the visual cortex are thought to be. They are relatively invariant to speed, contrast, and luminance, and these secondary parameters are encoded in separable functions [NDG$^+$11, WSH05], facilitating normalization through a population code at a future stage of processing.

The symmetries of the natural optic flow distribution constrain optimal direction selective neurons to prefer only the cardinal directions, as has been seen in On-Off DSRGCs [OB67]. This requirement means that direction selective tuning curves must also be orthogonal to one another, which has previously been shown to enable non-biased estimators of motion direction based on pairs of neurons [VH90]. The sharpness of tuning dramatically affects the information transmitted by the neural code, and the On-Off DSRGCs appear to have an optimal sharpness of tuning for this representation. A neuron receiving inputs from two orthogonally tuned neurons with similar receptive field positions would therefore have as much information as possible about the direction of motion at that position. It is currently unknown whether neurons receive input from two orthogonally tuned direction selective inputs, but the theory implies that such neurons could potentially be more reliable than neurons receiving either unidirectional or opposing inputs.

Information about direction selective neurons in the mouse LGN is limited to the superficial layer, where there appear to be direction selective neurons receiving inputs from either of the two horizontal directions, as well as receiving input from both opposing directions [MKNC12]. The theory predicts that a sharpening of tuning relative to the On-Off DSRGCs for pairs of opposing direction selective neurons. The pairs of horizontal direction selective LGN neurons appear to be significantly sharper than On-Off DSRGCs, in agreement with that prediction. The

colocalization of these neurons within the same region of the LGN, as well as this prediction, imply that the output of these neurons is optimal when considering a pair of neurons with opposing direction preferences at the same position. The subsequent processing of this information, either within the LGN or in visual cortex [RNG+11]., should therefore combine information across these colocalized classes of cells. The theory also predicts that vertical motion preferring cells should be significantly broader than the horizontal motion preferring cells. Together, these predictions suggest that the retinogeniculate motion circuit is highly optimized to carry information about the natural distribution of optic flows, in keeping with the efficient coding hypothesis.

Previous studies of optimal DS have primarily focused on either forced choice tasks [BSNM92] or the discriminability of stimuli [ZS99, SS93]. Brunel et al (1998) [BN98] showed that the mutual information can be derived from the Fisher Information under certain conditions, although Yarrow and Series (2012) [YS12] have showed that for small populations (as in the retinogeniculate circuit) they diverge. The Fisher Information does not allow for synergistic encoding schemes without additional terms and predicts an infinitely sharp tuning curve [ZS99, SS93]. The MI can be shown to reduce to the response entropy in the absence of noise - we further decompose it to observe dependence on the log Fisher Information, or line entropy. This result holds as well in the presence of additive Gaussian noise.

The observed shift from an optimal encoding of orthogonal to optimal encoding of oppositely tuned neurons fits our own data on the organization of mouse LGN [MKNC12], as well as historical studies that observed vertical motion preferring regions of rat LGN [MB69]. Futhermore, these results are consistent with the sharpening of a few driving inputs in the LGN in order to maximize information transmission through a more efficient encoding [SHS09]. However, our study differs from previous work in applying these ideas to the circuitry building motion features in the DSRGC pathway. It is presently unknown to what extent higher order motion features in the mouse exist and are derived from DSRGCs. As functional-anatomic methods reveal the subsequent stages of this motion circuit, the population encoding schemes described here can be extended to include larger

numbers of neurons and to generate novel hypothesis.

3.5 Materials and Methods

Optic flows were derived from the head mounted video of a cat walking in a natural environment [BEKK04] using the Lucas-Kanade algorithm. The distribution of optic flows $p(\theta)$ was summed across spatial positions and time points in the movie and then fit to a symmetric double exponential distribution given by

$$p(\theta) = K_1 + K_2 \exp\left[-\frac{|\theta - \pi i|}{K_3}\right] + K_4 \exp\left[-\frac{\left|\theta - \frac{\pi(2i+1)}{2}\right|}{K_5}\right], i \in 0, 1, \qquad (3.5)$$

and the goodness of fit was evaluated with the Pearson's correlation coefficient between the empirical distribution and the fit.

The mutual information between the empirical distribution of optic flows $p(\theta)$ was used to derive optimal direction selective tuning curves.

In order to observe how the sharpness of tuning affects the discriminability of direction selective tuning curves, the Fisher information ($\mathcal{F}$) for Gaussian noise around the response function,

$$\mathcal{F}(r, \theta) = r'(\theta)^2, \qquad (3.6)$$

was calculated. In order to ensure comparability between theoretical direction selective tuning curves and published On-Off DSRGC tuning curve parameters, von Mises response functions [EAG+08]),

$$r(\theta) = r_{max} \frac{\exp \kappa \cos(\theta - \theta_{max}}{\exp \kappa}, \qquad (3.7)$$

were used. κ, the sharpness of tuning, and θ_{max}, the preferred direction, were systematically varied in order to find the optimal preferred directions as a function of the sharpness of tuning. The average discriminability of timuli, $\langle \mathcal{F}(r(\theta)) \rangle_{p(\theta)}$, was used as the measure of optimal tuning in this section.

Optimal pairs of tuning curves were analyzed by fitting two separate von Mises response functions, with preferred directions $\theta_{max1} = \theta_{max2} + \epsilon$, where ϵ

was the angular distance between preferred directions. This distance was varied systematically, and the resulting pairwise mutual information was assessed in the low noise condition,

$$I(\vec{r};\theta) = H(\theta) + \underbrace{\frac{1}{2}\int d\theta p(\theta)\log[r_1'^2 + r_2'^2]}_{\text{Line entropy}} - \underbrace{\frac{1}{2}\log[2\pi e\sigma_r^2]}_{\text{Entropy of noise}}. \tag{3.8}$$

3.6 Appendix: Optimal tuning curves for axis selective cells

3.6.1 Introduction

Direction selective tuning curves can efficiently encode whether motion occurs in their preferred direction [i.e., $I(r;\delta\theta)$] only for the cardinal directions of motion. An underlying assumption of this theory is that neurons also wish to maximize the information contained about the stimulus direction ($I(r;\theta)$), and that $r(\theta)$ must be continuous. For direction selective tuning curves, all preferred directions can produce continuous tuning curves maximizing $I(r;\theta)$, but only the cardinal directions of motion could encode whether motion occurs in that direction optimally.

Here we generalize our theory to the case of bilateral symmetry, as is observed in axis of motion ($\phi = 2\theta \mod 2\pi$) encoding. We show that adaptive binning is necessary in order to generate tuning curves that maximize information about axis of motion ($I(r;\phi)$) for any axes of motion apart from horizontal and vertical. Adaptive binning of axes of motion leads to asymmetric axis tuning curves $r(\phi)$.

3.6.2 Results

Piecewise, the tuning curve $r(\theta)$ must locally match $|r'(\theta)|$ to $p(\theta)$ in order to achieve maximal response entropy. In order to be continuous, each of the n

piecewise segments must integrate to the same value,

$$\int_{a_1}^{a_2}(\theta)d\theta = \int_{a_2}^{a_3} p(\theta)d\theta = ... = \int_{a_{n-1}}^{a_n} p(\theta)d\theta = \frac{1}{n}. \tag{3.9}$$

Thus, direction selectivity is the special case where $n = 2$, so that each of the two segments integrates to $\frac{1}{2}$. Orientation selectivity is the case $n = 4$. This work considers the case where Δa is fixed, $a_2 - a_1 = a_3 - a_2 = ... = a_n - a_{n-1} = \Delta a$. The case where Δa is not fixed corresponds to adaptive binning, since the boundary points a_i are not at fixed distances from one another, but instead must be chosen to make the $\int_{a_i}^{a_{i+1}}(\theta)d\theta$ fixed.

The consequences of adaptive binning may be seen most clearly in the case of neurons which have tuning curves $r(\phi)$, where $\phi = 2\theta \mod 2\pi$. We will call these neurons axis selective, rather than orientation selective, to distinguish neurons responding to opposing directions of motion rather than stationary edges along a particular orientation, in keeping with [MKNC12]. That is, axis selective neurons are direction selective neurons defined on the doubled circle 2θ. $p(\phi)$ is bilaterally symmetric (Supplementary Figure 3.4A), whereas $p(\theta)$ is two-fold bilaterally symmetric (Figure 3.1A).

Direction selective tuning curves $r(\theta)$ that maximize $I(r;\theta)$ exist for all preferred directions θ_{max}, but they are asymmetric and do not maximize $I(r;\delta\theta)$ (Figure 3.1B). The symmetry constrains $a_2 = a_1 + \pi$ for all preferred directions, since each half of the distribution always has the same integral. Asymmetric tuning curves exist for neurons preferring directions other than the cardinal directions of motion, but this asymmetry constrains their optimality according to our theory.

Optimal axis selective tuning curves $r(\phi)$, in contrast, can only maximize $I(r;\phi)$ when either $\phi \in 0, \pi$ (horizontal or vertical motion) without adaptive binning (i.e, $a_2 = a_1 + \pi$). Any other orientation leads to $\int_{a_1}^{a_2} p(\theta)d\theta \neq \int_{a_2}^{a_3} p(\theta)d\theta$, as shown in Supplementary Figure S1C, so that the tuning curve is discontinuous. Adaptive binning creates the possibility of axis selective tuning curves maximizing $I(r;\phi)$ for all preferred axes (ϕ_{max}) (red curve; Supporting Figure S1C). The asymmetry of the adaptive binning tuning curves is systematically skewed towards the horizontal direction (circular-linear correlation between skewness of tuning curve

and preferred angle, $p<10^{-10}$), since the increased probability of horizontal motions leads to increased gain for those axes of motion. Thus, the optimal tuning curves for oblique angles have longer tails towards the vertical direction.

3.6.3 Discussion

The generalization of our theory provides insight into the relationship between adaptive binning of circular variables and the symmetries of the distribution of those variables. Adaptive binning is irrelevant to our analysis of optimal direction selective neurons, due to the two-fold bilateral symmetry of $p(\theta)$. Axis of motion selectivity, which we recently observe in the mouse LGN, is the encoding of a bilateral symmetric variable ϕ by monotonic tuning curves.

The theory presented here suggests that asymmetric tuning curves resulting from adaptive binning are necessary to encode any ϕ other than the horizontal and vertical axis. This result predicts that asymmetric tuning curves would exist for axis of motion selective neurons preferring oblique axes. Asymmetric tuning curves have been observed for orientation tuned neurons [HA78, Swi98], but axis of motion tuning differs from orientation tuning in that it represents pure selectivity for motion rather than combined edge/motion stimuli. Whereas two opposing cardinal direction selectivity inputs can be used to compute optimal axis selective tuning curves, optimal oblique axis of motion selective tuning curves would need to be computed de novo. The systematic asymmetry of oblique tuning curves is a clear prediction of this the generalized theory; if oblique axis of motion selective neurons are discovered, their tuning curves should be skewed away from the horizontal.

3.7 Figures

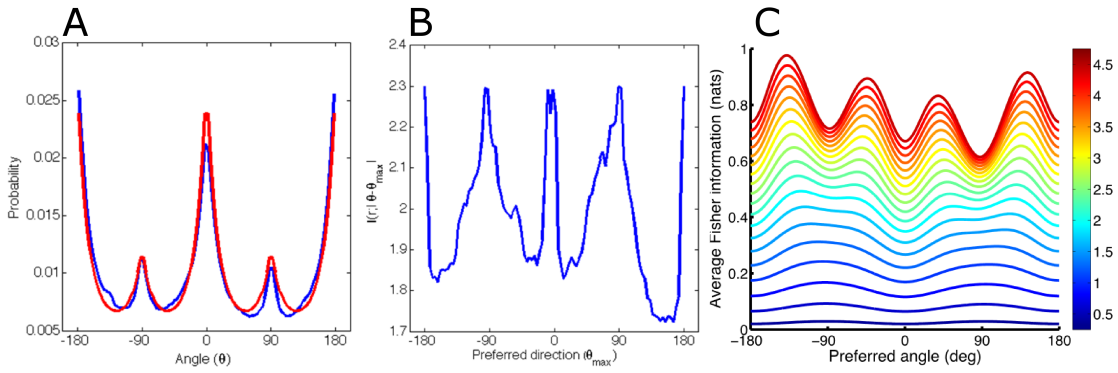

Figure 3.1: (A) Empirical distribution of optic flows (blue) derived from the CatCam video, showing local maxima and bilateral symmetry along the horizontal and vertical axes. The empirical distribution is well-fit by a symmetric double exponential (red; Materials and Methods). (B) Mutual information between neural response (r) and distance from preferred angle ($|\theta - \theta_{max}|$) for optimal direction selective neurons. Information can be maximized only when the preferred direction corresponds to an axis of symmetry of the stimulus distribution. Local maxima, representing optimal direction preferences, correspond to the horizontal and vertical directions. (C) Average Fisher Information for direction selective cells as a function of preferred direction preferring different directions, as a function of sharpness of tuning (κ). Overlay (dotted line) shows that the Fisher optimal prediction for direction preferences does not match the direction preferences of optimal direction selective neurons (B) from the mutual information.

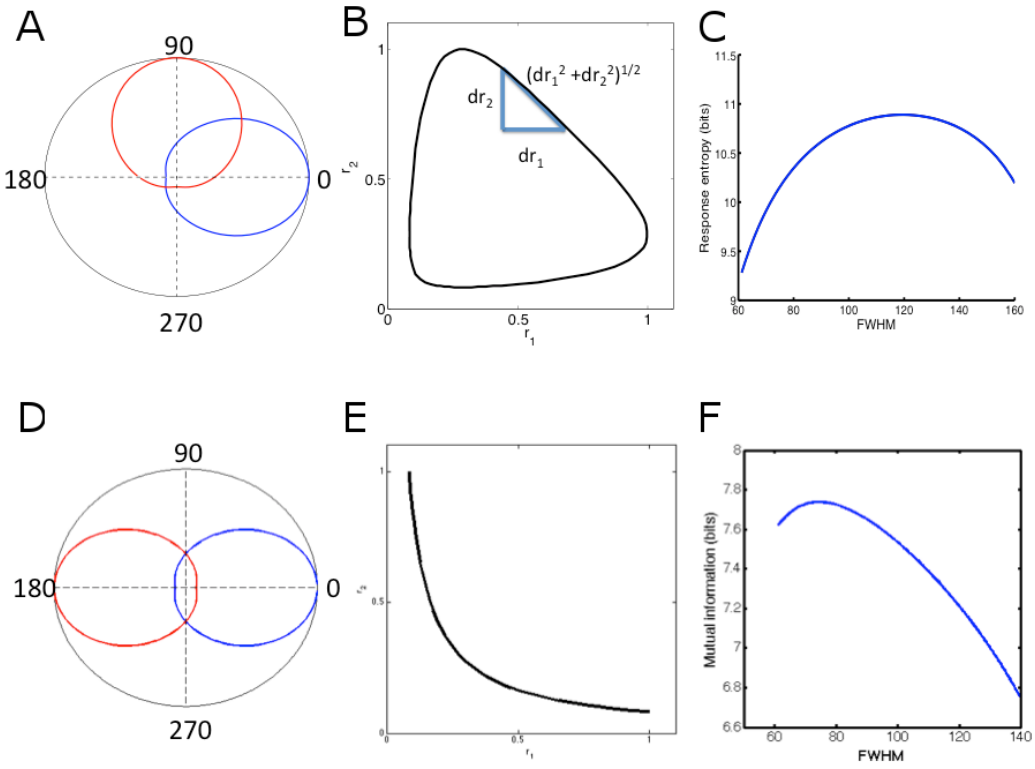

Figure 3.2: (A,D) Normalized firing rate tuning curve for two orthogonal direction preferring neurons, shown in red and blue (A) and two oppositely direction preferring neurons (D). The curves are von Mises response functions with a full width at half-maximum of 120°. (B,E) Trajectory in r_1-r_2 space corresponding to the orthogonal tuning curves (B) and opposite tuning curves (E). Diagram shows the arc-length along this trajectory, as in equation 4. (C,F) Response entropy (bits) has a clear maximum as a function of tuning width (FWHM) for orthogonal (C) and opposite (E) tuned cells. The maximum corresponds to the curves in A and B, and is very close to the tuning width observed for On-Off DSRGCs in the retina for orthogonal cells (C).

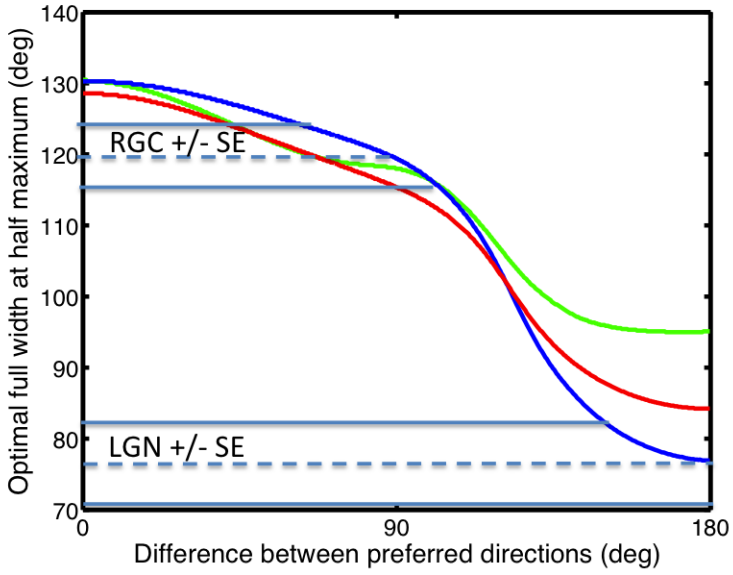

Figure 3.3: (A) Optimal direction selective tuning curve full-width at half-maximum as the angle between their preferred directions varies for horizontal (blue) and vertical (green) motion preferring cells with the natural scenes distribution or any direction under a uniform stimulus distribution

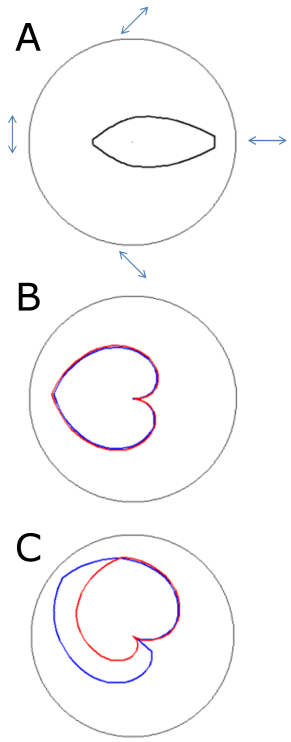

Figure 3.4: A. Black curve indicates the probability density of axis of motion for the natural scenes dataset, $p(\phi)$. Double-arrow labels indicate the axis of motion corresponding to ϕ: rightward is horizontal motion, leftward is vertical motion. B,C. Optimal axis of motion tuning curve ($|r'(\phi)| = p(\phi)$) derived as for direction selective cells is shown in blue for an axis preferring neuron (B: vertical axis prefering neuron, C: oblique angle axis preferring neuron). It is continuous for the vertical axis preferring curve in B and discontinuous for the oblique axis preferring neuron in C. Adaptive binning (as described in Supporting Text) derives a related optimal tuning curve, shown in red and offset slightly for visualization. The adaptive binning tuning curve is identical to the blue curve for the vertical axis preferring neuron (B), and differs from the blue curve for the oblique axis preferring neuron (C).

Chapter 3, in full, is a preprint of a paper that is being prepared for submission. Alfred P Kaye, Edward M Callaway, Tatyana O Sharpee. Optimal tuning curves for direction selective retinal ganglion cells. In Preparation, 2013. The dissertation author was the primary investigator and author of this paper.

Bibliography

[Adi85] Gilad Adiv. Determining Three-Dimensional motion and structure from optical flow generated by several moving objects. *Pattern Analysis and Machine Intelligence, IEEE Transactions on*, PAMI-7(4):384 –401, July 1985.

[AG00] Bagrat Amirikian and Apostolos P Georgopulos. Directional tuning profiles of motor cortical cells. *Neuroscience Research*, 36(1):73–79, January 2000.

[AO95] F.R. Amthor and C.W. Oyster. Spatial organization of retinal information about the direction of image motion. *Proceedings of the National Academy of Sciences*, 92(9):4002, 1995.

[App72] S Appelle. Perception and discrimination as a function of stimulus orientation: the "oblique effect" in man and animals. *Psychological bulletin*, 78(4):266–278, October 1972. PMID: 4562947.

[BEKK04] Belinda Y Betsch, Wolfgang Einhuser, Konrad P Krding, and Peter Knig. The world from a cat's perspective–statistics of natural videos. *Biological Cybernetics*, 90(1):41–50, January 2004. PMID: 14762723.

[BH63] Horace B Barlow and Richard M Hill. Selective sensitivity to direction of movement in ganglion cells of the rabbit retina. *Science*, 139(3553):412–412, February 1963.

[BHD11] Kevin L. Briggman, Moritz Helmstaedter, and Winfried Denk. Wiring specificity in the direction-selectivity circuit of the retina. *Nature*, 471(7337):183–188, March 2011.

[BL65] H B Barlow and W R Levick. The mechanism of directionally selective units in rabbit's retina. *The Journal of Physiology*, 178(3):477–504, June 1965. PMID: 5827909 PMCID: PMC1357309.

[BN98] Nicolas Brunel and Jean-Pierre Nadal. Mutual information, fisher information, and population coding. *Neural Computation*, 10(7):1731–1757, 1998.

[BR61] HB Barlow and WA Rosenblith. Possible principles underlying the transformations of sensory messages. In *Sensory Communication*, pages 217–234. MIT Press, 1961.

[BSNM92] K. H. Britten, M. N. Shadlen, W. T. Newsome, and J. A. Movshon. The analysis of visual motion: A comparison of neuronal and psychophysical performance. *The Journal of Neuroscience*, 12(12):4745–4765, December 1992.

[CDL71a] B G Cleland, M W Dubin, and W R Levick. Simultaneous recording of input and output of lateral geniculate neurones. *Nature: New biology*, 231(23):191–192, June 1971. PMID: 4325715.

[CDL71b] B G Cleland, M W Dubin, and W R Levick. Sustained and transient neurones in the cat's retina and lateral geniculate nucleus. *The Journal of physiology*, 217(2):473–496, September 1971. PMID: 5097609.

[CHS07] Matteo Carandini, Jonathan C. Horton, and Lawrence C. Sincich. Thalamic filtering of retinal spike trains by postsynaptic summation. *Journal of Vision*, 7(14), December 2007.

[CK90] C. E. Carr and M. Konishi. A circuit for detection of interaural time differences in the brain stem of the barn owl. *The Journal of Neuroscience*, 10(10):3227–3246, October 1990.

[CL07] Dirk Calow and Markus Lappe. Local statistics of retinal optic flow for self-motion through natural sceneries. *Network: Computation in Neural Systems*, 18(4):343–374, January 2007.

[CR00] C Chen and W G Regehr. Developmental remodeling of the retinogeniculate synapse. *Neuron*, 28(3):955–966, December 2000. PMID: 11163279.

[CRS03] Charles L Cox, Iva Reichova, and S Murray Sherman. Functional synaptic contacts by intranuclear axon collaterals of thalamic relay neurons. *The Journal of neuroscience: the official journal of the Society for Neuroscience*, 23(20):7642–7646, August 2003. PMID: 12930803.

[DHT+10] Daniel A Dombeck, Christopher D Harvey, Lin Tian, Loren L Looger, and David W Tank. Functional imaging of hippocampal place cells at cellular resolution during virtual navigation. *Nature neuroscience*, 13(11):1433–1440, November 2010. PMID: 20890294.

[DW91] C. J. Duffy and R. H. Wurtz. Sensitivity of MST neurons to optic flow stimuli. II. mechanisms of response selectivity revealed by small-field stimuli. *Journal of Neurophysiology*, 65(6):1346–1359, June 1991.

[EAG+08] Justin Elstrott, Anastasia Anishchenko, Martin Greschner, Alexander Sher, Alan M Litke, E J Chichilnisky, and Marla B Feller. Direction selectivity in the retina is established independent of visual experience and cholinergic retinal waves. *Neuron*, 58(4):499–506, May 2008. PMID: 18498732.

[EB89] M Egelhaaf and A Borst. Transient and steady-state response properties of movement detectors. *Journal of the Optical Society of America. A, Optics and image science*, 6(1):116–127, January 1989. PMID: 2921651.

[FE91] Daniel J. Felleman and David C. Van Essen. Distributed hierarchical processing in the primate cerebral cortex. *Cerebral Cortex*, 1(1):1–47, January 1991.

[FM00] David Ferster and Kenneth D. Miller. Neural mechanisms of orientation selectivity in the visual cortex. *Annual Review of Neuroscience*, 23(1):441–471, 2000.

[FMW02] Shelley I Fried, Thomas A Mnch, and Frank S Werblin. Mechanisms and circuitry underlying directional selectivity in the retina. *Nature*, 420(6914):411–414, November 2002. PMID: 12459782.

[FSSI79] Y Fukuda, I Sumitomo, M Sugitani, and K Iwama. Receptive-field properties of cells in the dorsal part of the albino rat's lateral geniculate nucleus. *The Japanese journal of physiology*, 29(3):283–307, 1979. PMID: 502088.

[GS10] D. Ganguli and E. P. Simoncelli. Implicit encoding of prior probabilities in optimal neural populations. *Adv. Neural Information Processing Systems 23 (NIPS*10)*, 23, 2010.

[GT03] Matthew S Grubb and Ian D Thompson. Quantitative characterization of visual response properties in the mouse dorsal lateral geniculate nucleus. *Journal of neurophysiology*, 90(6):3594–3607, December 2003. PMID: 12944530.

[HA78] P. Heggelund and K. Albus. Orientation selectivity of single cells in striate cortex of cat: The shape of orientation tuning curves. *Vision Research*, 18(8):1067–1071, 1978.

[Hee93] D. J. Heeger. Modeling simple-cell direction selectivity with normalized, half-squared, linear operators. *Journal of Neurophysiology*, 70(5):1885–1898, November 1993.

[HHC+04] James E Hamos, Van Horn, Susan C, Denis Raczkowski, and S. Murray Sherman. Synaptic circuits involving an individual retinogeniculate axon in the cat. *The Journal of Comparative Neurology*, 259(2):165–192, October 2004.

[HS76] S Hochstein and R M Shapley. Quantitative analysis of retinal ganglion cell classifications. *The Journal of physiology*, 262(2):237–264, November 1976. PMID: 994039.

[HS81] Berthold K.P. Horn and Brian G. Schunck. Determining optical flow. *Artificial Intelligence*, 17(13):185–203, August 1981.

[HW59] D.H. Hubel and T.N. Wiesel. Receptive fields of single neurones in the cat's striate cortex. *The Journal of physiology*, 148(3):574–591, 1959.

[HW61] D. H. Hubel and T. N. Wiesel. Integrative action in the cat's lateral geniculate body. *The Journal of Physiology*, 155(2):385–398.1, February 1961. PMID: 13716436 PMCID: PMC1359861.

[HW62] D. H. Hubel and T. N. Wiesel. Receptive fields, binocular interaction and functional architecture in the cat's visual cortex. *The Journal of Physiology*, 160(1):106–154.2, January 1962. PMID: 14449617 PMCID: PMC1359523.

[HWE+09] Andrew D. Huberman, Wei Wei, Justin Elstrott, Ben K. Stafford, Marla B. Feller, and Ben A. Barres. Genetic identification of an On-Off Direction-Selective retinal ganglion cell subtype reveals a Layer-Specific subcortical map of posterior motion. *Neuron*, 62(3):327–334, May 2009. PMID: 19447089 PMCID: PMC3140054.

[KABR10] Aaron M. Kerlin, Mark L. Andermann, Vladimir K. Berezovskii, and R. Clay Reid. Broadly tuned response properties of diverse inhibitory neuron subtypes in mouse visual cortex. *Neuron*, 67(5):858–871, September 2010. PMID: 20826316 PMCID: PMC3327881.

[KDlHK+11] Jeremy N Kay, Irina De la Huerta, In-Jung Kim, Yifeng Zhang, Masahito Yamagata, Monica W Chu, Markus Meister, and Joshua R Sanes. Retinal ganglion cells with distinct directional preferences differ in molecular identity, structure, and central projections. *The Journal of neuroscience: the official journal of the Society for Neuroscience*, 31(21):7753–7762, May 2011. PMID: 21613488.

[KGH05] Jason N. D. Kerr, David Greenberg, and Fritjof Helmchen. Imaging input and output of neocortical networks in vivo. *Proceedings of the National Academy of Sciences of the United States of America*,

102(39):14063–14068, September 2005. PMID: 16157876 PMCID: PMC1201343.

[KH96] Holger G. Krapp and Roland Hengstenberg. Estimation of self-motion by optic flow processing in single visual interneurons. *, Published online: 05 December 1996; | doi:10.1038/384463a0*, 384(6608):463–466, December 1996.

[KVD+91] J.J. Koenderink, A.J. Van Doorn, et al. Affine structure from motion. *JOSA A*, 8(2):377–385, 1991.

[KZMS10] In-Jung Kim, Yifeng Zhang, Markus Meister, and Joshua R. Sanes. Laminar restriction of retinal ganglion cell dendrites and axons: Subtype-specific developmental patterns revealed with transgenic markers. *The Journal of neuroscience : the official journal of the Society for Neuroscience*, 30(4):1452, January 2010. PMID: 20107072 PMCID: PMC2822471.

[KZY+08] In-Jung Kim, Yifeng Zhang, Masahito Yamagata, Markus Meister, and Joshua R. Sanes. Molecular identification of a retinal cell type that responds to upward motion. *Nature*, 452(7186):478–482, March 2008.

[Lau81] S Laughlin. A simple coding procedure enhances a neuron's information capacity. *Zeitschrift Fr Naturforschung. Section C: Biosciences*, 36(9-10):910–912, October 1981. PMID: 7303823.

[LDL+11] Yoan LeChasseur, Suzie Dufour, Guillaume Lavertu, Cyril Bories, Martin Deschnes, Ral Valle, and Yves De Koninck. A microprobe for parallel optical and electrical recordings from single neurons in vivo. *Nature Methods*, 8(4):319–325, 2011.

[Lev67] W. R. Levick. Receptive fields and trigger features of ganglion cells in the visual streak of the rabbit's retina. *The Journal of Physiology*, 188(3):285–307, February 1967. PMID: 6032202 PMCID: PMC1396015.

[LMMP59] J.Y. Lettvin, H.R. Maturana, W.S. Mcculloch, and W.H. Pitts. What the frog's eye tells the frog's brain. *Proceedings of the IRE*, 47(11):1940 –1951, November 1959.

[LOT69] W R Levick, C W Oyster, and E Takahashi. Rabbit lateral geniculate nucleus: sharpener of directional information. *Science (New York, N.Y.)*, 165(3894):712–714, August 1969. PMID: 5793977.

[LPF03] Baowang Li, Matthew R. Peterson, and Ralph D. Freeman. Oblique effect: A neural basis in the visual cortex. *Journal of Neurophysiology*, 90(1):204–217, July 2003.

[Mas87] D. N. Mastronarde. Two classes of single-input x-cells in cat lateral geniculate nucleus. i. receptive-field properties and classification of cells. *Journal of Neurophysiology*, 57(2):357–380, February 1987.

[Mas92] David N. Mastronarde. Nonlagged relay cells and interneurons in the cat lateral geniculate nucleus: Receptive-field properties and retinal inputs. *Visual Neuroscience*, 8(05):407–441, 1992.

[MB69] Vicente M. Montero and John F. Brugge. Direction of movement as the significant stimulus parameter for some lateral geniculate cells in the rat. *Vision Research*, 9(1):71–88, January 1969.

[MCSK04] Adi Mizrahi, Justin C. Crowley, Eran Shtoyerman, and Lawrence C. Katz. High-resolution in vivo imaging of hippocampal dendrites and spines. *The Journal of Neuroscience*, 24(13):3147–3151, March 2004.

[MDCL86] S Molotchnikoff, D Delaunais, C Casanova, and P Lachapelle. Influence of a local inactivation in the superior colliculus on lateral geniculate responses in rabbits. *Brain research*, 375(1):66–72, June 1986. PMID: 3719360.

[MKNC12] James H *Marshel, Alfred P *Kaye, Ian Nauhaus, and Edward M Callaway. Anterior-posterior direction opponency in the superficial mouse lateral geniculate nucleus. *Neuron*, 76(4):713–720, November 2012. PMID: 23177957.

[MU81] D. Marr and S. Ullman. Directional selectivity and its use in early visual processing. *Proceedings of the Royal Society of London. Series B. Biological Sciences*, 211(1183):151–180, March 1981.

[NC09] Jonathan J. Nassi and Edward M. Callaway. Parallel processing strategies of the primate visual system. *Nature Reviews Neuroscience*, 10(5):360–372, May 2009.

[NDG+11] Przemyslaw Nowak, Allan C Dobbins, Timothy J Gawne, Norberto M Grzywacz, and Franklin R Amthor. Separability of stimulus parameter encoding by on-Off directionally selective rabbit retinal ganglion cells. *Journal of Neurophysiology*, 105(5):2083–2099, May 2011.

[NKKH04] Axel Nimmerjahn, Frank Kirchhoff, Jason N. D. Kerr, and Fritjof Helmchen. Sulforhodamine 101 as a specific marker of astroglia in the neocortex in vivo. *Nature Methods*, 1(1):31–37, October 2004.

[NNC12] Ian Nauhaus, Kristina J. Nielsen, and Edward M. Callaway. Nonlinearity of two-photon ca2+ imaging yields distorted measurements of tuning for v1 neuronal populations. *Journal of Neurophysiology*, 107(3):923–936, February 2012.

[OB67] Clyde W Oyster and Horace B Barlow. Direction-Selective units in rabbit retina: Distribution of preferred directions. *Science*, 155(3764):841–842, February 1967.

[OTC72] Clyde W. Oyster, Ellen Takahashi, and Han Collewijn. Direction-selective retinal ganglion cells and control of optokinetic nystagmus in the rabbit. *Vision Research*, 12(2):183–193, February 1972.

[Oys68] C. W. Oyster. The analysis of image motion by the rabbit retina. *The Journal of Physiology*, 199(3):613–635, December 1968.

[PLF04] Matthew R. Peterson, Baowang Li, and Ralph D. Freeman. The derivation of direction selectivity in the striate cortex. *The Journal of Neuroscience*, 24(14):3583–3591, April 2004.

[PSS03] Thomas A Pologruto, Bernardo L Sabatini, and Karel Svoboda. ScanImage: flexible software for operating laser scanning microscopes. *BioMedical Engineering OnLine*, 2:13, May 2003. PMID: 12801419 PMCID: PMC161784.

[RB05] S. Roth and M.J. Black. On the spatial statistics of optical flow. In *Computer Vision, 2005. ICCV 2005. Tenth IEEE International Conference on*, volume 1, pages 42 – 49 Vol. 1, October 2005.

[REZW+11] Michal Rivlin-Etzion, Kaili Zhou, Wei Wei, Justin Elstrott, Phong L. Nguyen, Ben Barres, Andrew D. Huberman, and Marla B. Feller. Transgenic mice reveal unexpected diversity of on-off direction selective retinal ganglion cell subtypes and brain structures involved in motion processing. *The Journal of neuroscience : the official journal of the Society for Neuroscience*, 31(24):8760–8769, June 2011. PMID: 21677160 PMCID: PMC3139540.

[RNG+11] Nathalie L Rochefort, Madoka Narushima, Christine Grienberger, Nima Marandi, Daniel N Hill, and Arthur Konnerth. Development of direction selectivity in mouse cortical neurons. *Neuron*, 71(3):425–432, August 2011. PMID: 21835340.

[SBA03] Marcin Szwed, Knarik Bagdasarian, and Ehud Ahissar. Encoding of vibrissal active touch. *Neuron*, 40(3):621–630, October 2003.

[SBNM96] M. N. Shadlen, K. H. Britten, W. T. Newsome, and J. A. Movshon. A computational analysis of the relationship between neuronal and behavioral responses to visual motion. *The Journal of Neuroscience*, 16(4):1486–1510, February 1996.

[SCM71] D L Stewart, K L Chow, and R H Masland. Receptive-field characteristics of lateral geniculate neurons in the rabbit. *Journal of neurophysiology*, 34(1):139–147, January 1971. PMID: 5540575.

[SG98] S. Murray Sherman and R. W. Guillery. On the actions that one nerve cell can have on another: Distinguishing drivers from modulators. *Proceedings of the National Academy of Sciences of the United States of America*, 95(12):7121–7126, June 1998. PMID: 9618549 PMCID: PMC22761.

[SGHK03] Christoph Stosiek, Olga Garaschuk, Knut Holthoff, and Arthur Konnerth. In vivo two-photon calcium imaging of neuronal networks. *Proceedings of the National Academy of Sciences of the United States of America*, 100(12):7319–7324, June 2003. PMID: 12777621.

[SH98] E.P. Simoncelli and D.J. Heeger. A model of neuronal responses in visual area mt. *Vision research*, 38(5):743–761, 1998.

[SHS09] Lawrence C Sincich, Jonathan C Horton, and Tatyana O Sharpee. Preserving information in neural transmission. *The Journal of Neuroscience*, 29(19):6207–6216, May 2009.

[SS93] H S Seung and H. Sompolinsky. Simple models for reading neuronal population codes. *Proceedings of the National Academy of Sciences*, 90(22):10749–10753, November 1993.

[Swi98] N.V. Swindale. Orientation tuning curves: empirical description and estimation of parameters. *Biological Cybernetics*, 78(1):45–56, 1998.

[TLZL94] K G Thompson, A G Leventhal, Y Zhou, and D Liu. Stimulus dependence of orientation and direction sensitivity of cat LGNd relay cells without cortical inputs: a comparison with area 17 cells. *Visual neuroscience*, 11(5):939–951, October 1994. PMID: 7947407.

[URR99] W M Usrey, J B Reppas, and R C Reid. Specificity and strength of retinogeniculate connections. *Journal of neurophysiology*, 82(6):3527–3540, December 1999. PMID: 10601479.

[VH90] J.H. Van Hateren. Directional tuning curves, elementary movement detectors, and the estimation of the direction of visual movement. *Vision Research*, 30(4):603–614, 1990.

[VM91] J D Victor and J Mast. A new statistic for steady-state evoked potentials. *Electroencephalography and clinical neurophysiology*, 78(5):378–388, May 1991. PMID: 1711456.

[VPM+10] Joshua T Vogelstein, Adam M Packer, Timothy A Machado, Tanya Sippy, Baktash Babadi, Rafael Yuste, and Liam Paninski. Fast nonnegative deconvolution for spike train inference from population calcium imaging. *Journal of neurophysiology*, 104(6):3691–3704, December 2010. PMID: 20554834.

[VT10] Sowmya Venkataramani and W Rowland Taylor. Orientation selectivity in rabbit retinal ganglion cells is mediated by presynaptic inhibition. *The Journal of neuroscience: the official journal of the Society for Neuroscience*, 30(46):15664–15676, November 2010. PMID: 21084622.

[WH88] William H. Warren and Daniel J. Hannon. Direction of self-motion is perceived from optical flow. *, Published online: 10 November 1988; | doi:10.1038/336162a0*, 336(6195):162–163, November 1988.

[WHZF11] Wei Wei, Aaron M. Hamby, Kaili Zhou, and Marla B. Feller. Development of asymmetric inhibition underlying direction selectivity in the retina. *Nature*, 469(7330):402–406, January 2011.

[WSH05] Shijun Weng, Wenzhi Sun, and Shigang He. Identification of ONOFF Direction-Selective ganglion cells in the mouse retina. *The Journal of Physiology*, 562(3):915–923, February 2005.

[WVS+11] Xin Wang, Vishal Vaingankar, Cristina Soto Sanchez, Friedrich T Sommer, and Judith A Hirsch. Thalamic interneurons and relay cells use complementary synaptic mechanisms for visual processing. *Nature neuroscience*, 14(2):224–231, February 2011. PMID: 21170053.

[YIS+09] Keisuke Yonehara, Hiroshi Ishikane, Hiraki Sakuta, Takafumi Shintani, Kayo Nakamura-Yonehara, Nilton L Kamiji, Shiro Usui, and Masaharu Noda. Identification of retinal ganglion cells and their projections involved in central transmission of information about upward and downward image motion. *PloS one*, 4(1):e4320, 2009. PMID: 19177171.

[YS12] S. Yarrow and P. Series. Fisher and shannon information in nite neural populations. *Cosyne*, 2012.

[ZS99] Kechen Zhang and Terrence J. Sejnowski. Neuronal tuning: To sharpen or broaden? *Neural Computation*, 11(1):75–84, 1999.